Bur1 functions with TORC1 for vacuole-mediated cell cycle progression

Yui Jin[1,2,3,*], Natsuko Jin[3,¶], Yu Oikawa[2], Ron Benyair[3], Michiko Koizumi[2], Thomas E. Wilson[4], Yoshinori Ohsumi[1,2,*], and Lois S. Weisman[3,5,*]

[1]Tokyo Tech World Research Hub Initiative (WRHI)

[2]Cell Biology Center, Institute of Innovative Research, Tokyo Institute of Technology, Japan

[3]Life Sciences Institute, University of Michigan, USA

[4]Department of Pathology, University of Michigan, USA

[5]Department of Cell and Developmental Biology, University of Michigan, USA

¶ Present address: Live Cell Super-Resolution Imaging Research Team, RIKEN Center for Advanced Photonics, Wako, Saitama, Japan.

* Co-corresponding authors

Lead author: Lois S. Weisman

Running title: Roles for Bur1 in cell cycle progression

Key words: lysosome; rapamycin; *SGV1; SCH9*; yeast

Character count: 24,743

Abstract

The vacuole/lysosome plays essential roles in the growth and proliferation of many eukaryotic cells via the activation of target of rapamycin complex 1 (TORC1). Moreover, the yeast vacuole/lysosome is necessary for progression of the cell division cycle, in part via signaling through the TORC1 pathway. Here we show that an essential cyclin-dependent kinase, Bur1 plays critical roles in cell-cycle progression in cooperation with TORC1. A mutation in *BUR1* combined with a defect in vacuole inheritance shows a synthetic growth defect. Importantly, the double mutant, as well as a *bur1-267* mutant on its own, has a severe defect in cell-cycle progression from G_1 phase. In further support that *BUR1* functions with TORC1, mutation of *bur1* alone results in high sensitivity to rapamycin, a TORC1 inhibitor. Mechanistic insight for Bur1 function comes from the findings that Bur1 directly phosphorylates Sch9, a target of TORC1 and that both Bur1 and TORC1 are required for the activation of Sch9. Together, these discoveries suggest that multiple signals converge on Sch9 to promote cell-cycle progression.

Introduction

The presence of organelles is a defining feature of eukaryotic cells, and organelles play multiple critical roles within the cell. As essential compartments of cell function, organelle inheritance pathways ensure the presence of functional organelles in the resultant daughter cell after cell division (Jin and Weisman, 2015). The budding yeast *Saccharomyces cerevisiae* is an excellent model system to study the coordination of organelle dynamics and the cell cycle because the cell division of budding yeast is asymmetric. The nature of asymmetric division requires active, and regulated organelle transport in each cell cycle. In budding yeast, organelles are generally transported from mother to daughter cells (Weisman, 2006; Knoblach and Rachubinski, 2015).

Previously, we assessed the mechanism and regulation of vacuole inheritance as an example of an organelle that is actively transported during the cell cycle (Weisman, 2006). The vacuole is involved in a number of specialized cellular processes, including protein degradation, storage of nutrients, and protection from stress (Klionsky *et al.*, 1990; Ohsumi, 2006; Jin *et al.*, 2017) During cell division in budding yeast, vacuoles are transported from mother cells to daughter cells by the vacuole transport complex, which is comprised of the myosin V motor Myo2, the vacuole membrane anchored protein Vac8, and a vacuole-specific adaptor protein Vac17 which links Myo2 and Vac8 on the vacuole membrane (Catlett and Weisman,

1998; Wang *et al.*, 1998; Ishikawa *et al.*, 2003). When vacuole inheritance is defective, vacuoles can be generated *de novo* in the bud (daughter cell), but these newly synthesized vacuoles are much smaller than normal vacuoles, and lack some functions (Anand *et al.*, 2009; Jin and Weisman, 2015). The small vacuoles eventually grow to a normal size and regain full function likely by acceleration of a pathway that contributes to the *de novo* synthesis of the vacuole.

In an genome wide *s*ynthetic *g*enetic *a*rray (SGA) analysis (Costanzo *et al.*, 2010), 5.4 million gene-gene double knock-out strains were generated and their phenotypes were reported. Of these, over twenty genes were proposed to be synthetically lethal with the vacuole inheritance defective, *vac17Δ* mutant. When tested further, three types of double mutants *vac17Δ pep12Δ*, *vac17Δ vps45Δ*, and *vac17Δ tor1Δ* displayed synthetic growth defects (Jin and Weisman, 2015). In addition, the disruption of *PEP12*, *VPS45*, or *TOR1* loci resulted in a synthetic growth defect with other vacuole inheritance mutants, *vac8Δ*, and *myo2-N1304D*, which are deficient in the association of the vacuole with Myo2 (Eves *et al.*, 2012). Notably, in the complete absence of vacuole inheritance, *PEP12* and *VPS45* are required for the *de novo* synthesis of the vacuole, and that the newly formed vacuoles need to mature and then signal through *TOR1* for progression of cell cycle in G_1 phase (Jin and Weisman, 2015). *TOR1* is also required for the G_1-S transition (Moreno-Torres *et al.*, 2015).

It was not known whether in addition to TORC1, any other pathway that signals from the vacuole, is required for G_1 progression. Here we performed a genetic screen and found that *BUR1* is also critical for G_1 progression. *BUR1* is an essential gene, and encodes a cyclin-dependent kinase CDK, whose cyclin partner is Bur2 (Yao *et al.*, 2000). The Bur1-Bur2 complex regulates transcriptional elongation through phosphorylation of the C-terminal domain (CTD) of RNA polymerase II (Pol II) (Yao *et al.*, 2000; Murray *et al.*, 2001; Keogh *et al.*, 2003). Compared to other CDKs, Bur1 has a tail that extends C-terminally from the kinase domain. While *BUR1* is an essential gene, the C-terminal tail is not essential for growth under normal conditions (Irie *et al.*, 1991; Prelich and Winston, 1993; Clausing *et al.*, 2010). The C-terminal tail of Bur1 interacts with Rfa1 (Clausing *et al.*, 2010), and the C-terminal deletion causes high sensitivity to several drugs, such as 6-azauracil (6-AU), methyl methanesulfonate (MMS) and hydroxyurea (HU), which induce impaired

transcription, DNA damage and replication stress, respectively. In addition, Bur1 was predicted to be involved in cell cycle progression during adaptation to the pheromone response, however how Bur1 affects the cell cycle during this adaption was unclear (Irie *et al.*, 1991; Prelich and Winston, 1993). Here we link Bur1 to the basal cell cycle by discovering that Bur1 mutants have defects in cell-cycle progression, and that Bur1 directly phosphorylates Sch9, a known target of TORC1 (Urban *et al.*, 2007). Importantly, TORC1 phosphorylation of Sch9 on the vacuole is essential for cell-cycle progression (Jin *et al.*, 2014). Together, we propose that kinase signaling pathways are critical for cell cycle progression in G_1 phase, and that Sch9 is likely a hub for these pathways.

Results

Mutation of *BUR1* combined with mutations in vacuole inheritance exhibit synthetic growth defects

To further uncover mechanisms for vacuole-mediated cell cycle progression, we performed a synthetic lethal screen with the *vac17*Δ mutant, using a color sectoring assay (Keppler-Ross et al., 2008). We used a *URA3* based multi-copy (2μ) plasmid that encodes mCherry fluorescent protein modified for optimized yeast codon usage (Keppler-Ross *et al.*, 2008), and *VAC17*. The resultant plasmid was transformed into a *vac17*Δ strain (Fig. 1A). Note that a *vac17Δ* mutant on its own is viable (Ishikawa *et al.*, 2003), thus a *vac17*Δ mutant still grows following loss of the *VAC17* containing plasmid. We then performed EMS mutagenesis. We selected for strains that could not lose the plasmid even on non-selective medium. Of the 13,000 colonies examined, we identified seven mutants that could not lose the plasmid. Six out of seven mutants had a mutation in *TOR1*, which was previously shown to be synthetically lethal with *vac17Δ*; this demonstrates the effectiveness of the screen.

To identify the corresponding gene of the remaining mutant, we performed whole genome sequencing (Birkeland *et al.*, 2010) and identified a mutation in *BUR1/SGV1, bur1-W267stop* (named *bur1-267*) (Fig. 1, B and C). The *bur1-267* mutant has a stop codon at residue W267, resulting in a deletion of the C-terminal tail plus one third of the kinase domain (Fig. 1B). When assessed by a tetrad dissection assay, the *bur1-267 vac17*Δ double mutant showed a worse growth defect compared with the *bur1-267* mutant alone (Fig. 1, D and E). This large deletion suggests that the *bur1-267* mutant has defects in *BUR1* functions, Thus, we also analyzed the *bur1-ΔC*

(Δ373-657) mutant (Clausing *et al.*, 2010) which retains the entire kinase domain, but lacks the C-terminal region of the Bur1 protein. Note that the C-terminal region of Bur1 is not essential for growth under normal condition (Clausing *et al.*, 2010) (Fig. 1, F and G).

Importantly, the *bur1-ΔC* mutant exhibited a synthetic growth defect with *vac17*Δ (Fig. 1, F-H). We found that the *bur1-ΔC* also exhibited a synthetic growth defect with other vacuole inheritance mutants, *vac8*Δ and *myo2-N1304D* (Fig. EV1, A and B). These findings indicate that Bur1 is critical for growth in the absence of vacuole inheritance, and also raises the possibility that the C-terminus of Bur1 has a positive role in vacuole-mediated cell cycle progression.

Bur1 CDK is involved in vacuole-mediated cell cycle progression

In an earlier study, we found that both *pep12-60 vac17*Δ and *tor1*Δ *vac17*Δ double mutants show a delay in G_1 progression (Jin and Weisman, 2015). To test whether the *bur1-ΔC vac17*Δ double mutant also exhibits a cell cycle delay in G_1, we utilized flow cytometry to assess DNA content. We found that wild-type (WT), *bur1-ΔC*, or the *vac17*Δ mutant each had similar distribution of cells in G_1 phase (1N DNA) vs. G_2 phase (2N DNA), indicating that these mutants exhibit normal cell cycle progression (Fig. 2, A and B). In contrast, the *bur1-ΔC vac17*Δ double mutant showed an increase in cells in G_1 phase (1N DNA) and a concomitant decrease in cells in G_2 phase (2N DNA) (Fig. 2, A and B), consistent with a delay in exit from G_1 phase.

To further test whether Bur1 is important for G_1 progression when vacuole inheritance is normal, we assessed the *bur1-267* mutant and found that there was an increase in cells in G_1 phase as measured by flow cytometry analysis (Fig. 2, C and D). This indicates that mutation of *BUR1* alone results in a defect in cell-cycle progression from G_1 phase.

We also took an orthogonal approach to monitor cell-cycle progression through G_1 phase. Whi5, a repressor of G_1 transcription, is cytoplasmic during most of the cell-cycle and localizes in the nucleus at early G_1 phase (Costanzo *et al.*, 2004; de Bruin *et al.*, 2004). Whi5 nuclear localization is transient and released by Cdc28-Cln3 activity, which enables progression through early G_1 phase. Thus, we used the localization of Whi5 to monitor the number of cells in early G_1 phase. We found that the *bur1-ΔC vac17*Δ double mutant exhibited more cells with Whi5 in the nucleus, 40%, of cells with Whi5, compared with WT, *vac17Δ,* or *bur1-*ΔC, which had lower

percentages of cells with Whi5 in the nucleus; 23%, 24%, and 25%, respectively (Fig. 2, E and F). These results suggest that the *bur1-ΔC vac17Δ* double mutant exhibits a delay in progression through G_1 phase. Notably, in the *bur1-267* mutant, there was also an increase in cells in G_1 phase as measured by Whi5 localization in the nucleus (Fig. EV2, A and B). These data suggest that similar to TORC1, *BUR1* is required for cell cycle progression through G_1 phase.

Previously, we showed that a *pep12-60 vac17Δ* double mutant is defective in cell-cycle progression through G_1 phase at the restrictive temperature and is also defective in *de novo* synthesis of a vacuole in the bud. In contrast, the *tor1Δ vac17Δ* double knockout strain, which also exhibits a delay in G_1 phase, is not defective in producing a new vacuole (Jin and Weisman, 2015). We showed that these phenotypes occurred because 1) a mature vacuole plus 2) signaling via Tor1 and Sch9 from the mature vacuole is required for progression through G_1 phase. To determine whether the *bur1-ΔC vac17Δ* double mutant is defective in either or both pathways, we first tested whether this mutant has a defect in the *de novo* synthesis of the vacuole. We used Vph1-GFP to label all vacuoles and FM4-64 to monitor inherited vacuoles. Wild-type and *bur1-ΔC* cells showed normal vacuole inheritance (Fig. 3A). Instead, *bur1-ΔC vac17Δ* as well as *vac17Δ* cells showed a vacuole inheritance defect and produced new vacuoles, which were FM4-64 negative but Vph1-GFP positive vacuoles (Fig. 3B). Thus, in the absence of vacuole inheritance, the *bur1-ΔC vac17Δ* mutant is able to synthesize a new vacuole. These findings suggest that *bur1-ΔC vac17Δ* cells have a defect in signaling from the vacuole.

***BUR1* functions in parallel with the TORC1 pathway.**

That the *bur1-ΔC vac17Δ* and *tor1Δ vac17Δ* double mutants show similar phenotypes (Figs 1, 2 and 3)(Jin and Weisman, 2015), raised the possibility that Bur1 and TORC1 function in the same pathway(s). To further elucidate a potential relationship between Bur1 and TORC1, we tested whether *in vivo*, Bur1 affects the phosphorylation status of Sch9, which is a TORC1 target. In a gel shift assay, compared with WT cells, the *bur1-ΔC vac17Δ* double mutant showed a decrease in phosphorylation of Sch9 (Fig. 4A, and Fig. EV3A). To further test if this phosphorylation specifically requires Bur1 whether or not vacuole inheritance is defective, we performed a gel shift assay comparing Sch9 in a WT strain vs. a *bur1-267* mutant, a *vac17Δ* mutant, and a *bur1-267 vac17Δ* double mutant. We found a

decrease in Sch9 phosphorylation in both the *bur1-267* mutant, and the *bur1-267 vac17Δ* double mutant (Fig. 4B and Fig. EV3A). These results indicate that Bur1 plays a role in the phosphorylation of Sch9 *in vivo*.

To further test if Bur1 functions in the same pathway as Tor1, we tested another *tor1*Δ phenotype, increased sensitivity to rapamycin (Lorenz and Heitman, 1995). We found that similar to the *tor1*Δ mutant, the *bur1-ΔC* mutant also exhibits an increased sensitivity to rapamycin (Fig. 4C). Moreover, the *tor1*Δ *bur1-ΔC* double mutant was even more sensitive to rapamycin compared with either single mutant alone (Fig. 4C). These results strongly suggest that Bur1 and Tor1 function together in the TORC1 pathway. In support of this, we found that *TOR1* over expression rescued both the growth defect of a *bur1-ΔC vac17*Δ double mutant (Fig. EV3B), and the rapamycin sensitivity of *bur1-ΔC* and *bur1-ΔC vac17*Δ mutants (Fig. EV3C). In contrast, over-expression of *BUR1* and *BUR2* did not rescue the growth defect of a *tor1*Δ *vac17*Δ double mutant (Fig. EV3, D and E). Taken together, these results strongly suggest that for its role in the cell cycle, *BUR1* functions in parallel, but not downstream of *TOR1*, and is involved in the TORC1 pathway through the phosphorylation of Sch9.

The Bur1 kinase associates and phosphorylates Sch9

To test whether Bur1 associates with Sch9, we used recombinant proteins and performed pull-down experiments from yeast lysates. Recombinant GST-Sch9 (1-390) and GST-Sch9 (391-824), but not GST alone, pulled down Bur1 from yeast lysates (Fig. EV4A). Next, we addressed whether Bur1 directly phosphorylates Sch9, and performed *in vitro* protein kinase assays using radio-labeled γ^{32}P-ATP. Bur1 was immunoprecipitated from yeast lysates and bacterially expressed GST-Sch9 was utilized as the substrate (Fig. 5, A and B). We found that the C-terminal region of Sch9 (391-824), but not the N-terminus (1-390), was phosphorylated in a Bur1-dependent manner *in vitro* (Fig. 5B, lanes 4 and 6). The fact that only the C-terminal half of Sch9 was phosphorylated *in vitro*, suggests that this *in vitro* assay reflects the substrate specificity of Bur1. Moreover, we found that Bur1, but not Bur1-ΔC, phosphorylated itself *in vitro* (Fig. 5B, lanes 2, 4, 6 and 8, 10, 12) (Yao *et al.*, 2000; Murray *et al.*, 2001). Note that Bur1-ΔC had much less kinase activity on Sch9 *in vitro* compared with wild-type Bur1 (Fig. 5B, lanes 4 and 10). However, Bur1-ΔC bound to GST-Sch9 (391-824) (Fig. EV4A). Together, these results suggest that Bur1

directly associates and phosphorylates Sch9 *in vivo*, and that the C-terminal region of Bur1 is important for phosphorylation of Sch9 and of itself. Those results suggest that C-terminus of Bur1 is required for its kinase activity, but not for association with kinase substrate(s) including Sch9. Notably, over-expression of the C-terminal region did not inhibit a growth of wild-type yeast (Fig. EV4B). Moreover, over-expression of the region did not change the rapamycin sensitivity of the *bur1-ΔC* mutant (Fig. EV4, C and D). That the C-terminal region of Bur1 is dispensable under normal conditions, suggests that the C-terminal region of Bur1 is required for efficient phosphorylation of Sch9. These findings further suggest that Bur1 has at least two roles: one that is potentially for known transcription regulation at the nucleus, which does not require its C-terminal region, and a second role(s) that requires the Bur1 C-terminus and is required for the vacuole-mediated pathway.

To gain molecular insight into Bur1-dependent phosphorylation of Sch9 during cell cycle progression, we used mass-spectrometry analysis to determine residues on Sch9 that are phosphorylated by Bur1 *in vitro.* We identified eleven serine/threonine residues in Sch9 that are phosphorylated by Bur1: S560, T568/T570/T574/T575, S709/T710/S711, T721/T723, and S726 (Fig. 5C) (Table 1). Note that while two of these sites (T723P and S726P) match with the canonical CDK kinase motif, S/P or T/P, many of the other sites do not match this consensus. However, note that Bur1 was previously shown to phosphorylate non-canonical sites. None of the Bur1 sites in Spt5 contain an S/P or T/P motif (Liu *et al.*, 2009). Moreover, other CDK also use both canonical and non-canonical sites. For example, Cdk1 sites that do not contain S/P or T/P have also been identified (Suzuki *et al.*, 2015).

To address the physiological importance of Bur1-dependent phosphorylation of Sch9, we tested the putative Bur1 target sites on Sch9, except for T570 and T574. T570 which is in the activation loop of the Sch9 kinase domain, is also a Pkh1/2 site, and was previously shown to be essential for Sch9 function (Urban *et al.*, 2007). T574 is also highly conserved in the activation loop of many AGC kinases (Jacinto and Lorberg, 2008). We substituted all nine remaining Thr/Ser Bur1 phosphorylation sites, with non-phosphorylatable alanine. The resultant Sch9-9A mutant did not support the growth of *sch9Δ* cells (Fig. EV4E), which suggests that phosphorylation

of at least a subset of sites are critical for yeast growth. Note that while seven of these sites have not been reported previously as Bur1 sites, two of these, T723 and S726, were previously identified as TORC1 sites, and were changed to phosphomimetic mutations in the Sch9-2D3E $^{(T723D, 726D \text{ with } T737E, S758E, S765E)}$ mutant (Urban *et al.*, 2007). This suggests that Bur1 and TORC1 phosphorylate overlapping sites, yet each also phosphorylates unique, essential sites. In support of this, we found that over-expression of the phosphomimetic Sch9-2D3E mutant which is constitutively active in absence of TORC1 activity, did not suppress the growth defect of a *bur1*-Δ*C vac17*Δ double mutant (Fig. EV4F).

One of the predicted Bur1 sites on Sch9, S711, was specifically shown to not be phosphorylated by TORC1 or Pkh1/2 (Urban *et al.*, 2007). Thus, we generated a Sch9 allele where T711 as well as two additional adjacent Bur1-dependent phosphorylation sites were mutated, S709A, T710A, and T711A, and found that this *sch9-3A* mutant exhibited a growth defect (Fig. EV4E). In addition, the phospho-mimetic Sch9-3D/E $^{(S709E, T710D, T711E)}$ mutant showed a similar growth defect in *sch9-3A* cells and did not rescue the growth defect of the *bur1*-Δ*C vac17*Δ double mutant (Fig. EV4F). These observations suggest that phosphorylation of these three sites are not sufficient for full function of Sch9 *in vivo*. Alternatively, the substitutions of aspartic and glutamic acids at these specific sites may not fully mimic phosphorylation. Importantly, that mutation of just these three sites caused a growth defect, provides additional support to the hypothesis that these sites, which are not TORC1 and Pkh1/2 sites, are required for Sch9 activation by Bur1-Bur2, and function in Bur1-dependent cell cycle progression.

That Bur1-dependent, but TORC1-independent sites on Sch9 are critical for Sch9 function, strongly suggests that TORC1 and Bur1 act in parallel, and that both kinases are critical for Sch9 phosphorylation. Indeed, phospho-mimetic Sch9-2D3E combined with S709A, T710A, and T711A (Sch9-3A-2D3E) did not rescue the rapamycin sensitivity of *tor1*Δ or *bur1*-Δ*C* mutant, while Sch9-2D3E partially rescued the sensitivity of *tor1*Δ (Fig. 5, D and E). Note that over-expression of the phospho-mimetic Sch9-3D/E as well as Sch9-3D/E combined with 2D3E (Sch9-3D/E-2D3E) did not rescue the rapamycin sensitivity of *bur1*-Δ*C* (Fig. 5E).

Bur1 functions at the nucleus for TORC1 pathway

Bur1-dependent regulation of transcription occurs in the nucleus (Yao *et al.*, 2000; Murray *et al.*, 2001; Keogh *et al.*, 2003). However, it is unknown where Bur1 functions for vacuole-mediated cell cycle progression. To monitor the cellular localization of Bur1, we used mNeonGreen fused to Bur1 (Bur1-mNG) (Shaner *et al.*, 2013). As previously reported, Bur1-mNG mainly localized to the nucleus (Fig. EV5A) (Huh *et al.*, 2003). However, a portion of Bur1 is found in the cytoplasm (Fig. EV5, A and B). Interestingly, when compared with wild-type Bur1, Bur1-ΔC had a reduced cytoplasmic localization (Fig. EV5, A and B). This was not due to lower expression of Bur1-ΔC (Fig. EV5C), which suggests that Bur1-ΔC does not retain the cytoplasmic functions of wild-type Bur1. This raises the possibility that Bur1 has at least two functions, one in the nucleus, the other in the cytoplasm.

To determine whether the cytoplasmic pool of Bur1 changes during cell-cycle, we synchronized yeast cell-cycle using alpha-mating factor arrest and release. There was not a dramatic change in the cytoplasmic pool of Bur1 during the cell cycle. However, we observed an increase in nuclear Bur1 at 120 minutes after release from alpha-factor arrest, which corresponds to the second initiation of the cell-cycle (Fig. EV5D). This is consistent with the possibility that Bur1 has a nuclear role early in the cell-cycle. Note that the initial release of cells from alpha-factor is not identical to G1 phase in asynchronous cells, while initiation of the second cell-cycle is closer to G1 phase in asynchronous cells.

To further probe the importance of Bur1 localization to the nucleus, we mutated a predicted importin α-dependent nuclear-localization signal (NLS) (14-49 aa) in Bur1 (Kosugi *et al.*, 2009). Deletion of an N-terminal region (2-49 aa) of Bur1 (Bur1-ΔN) results in much less Bur1 in the nucleus (Fig. EV5E). Importantly, while this mutant supports yeast growth under normal conditions (Fig. EV5 F), the Bur1-ΔN did not fully support rapamycin sensitivity of *bur1-ΔC* (Fig. 6, A and B). These results suggests that Bur1 functions in the nucleus at some point during TORC1 activation. In support of this, we found that Bur1 fused to the SV40-NLS (Kalderon *et al.*, 1984) showed a similar degree of rapamycin sensitivity compared with wild-type Bur1 (Fig. 6A). In contrast, adding a nuclear-export signal (NES) of PKI (Wen *et al.*, 1995) to Bur1 resulted in higher rapamycin sensitivity compared to Bur1 without the NES (Fig. 6B). Moreover, a combination of a deletion of the importin α-dependent

NLS plus the addition of PKI-NES showed much more sensitivity to rapamycin (Fig. 6B). These results suggest that some nuclear functions of Bur1 are required for the activation of the TORC1 pathway.

That *bur1* mutants have synthetic phenotypes with vacuole inheritance mutants, suggests that some of the functions of Bur1 occur on the vacuole membrane. Taken together we propose that progression of the cell-cycle requires Bur1 functions in the cytoplasm and nucleus, which includes the phosphorylation of Sch9, as well as TORC1 phosphorylation of Sch9 in the cytoplasm. Moreover, at least some of these events likely occur specifically on the vacuole membrane.

Discussion

Here we discovered that when cells do not receive a mature vacuole from the mother cell, Bur1 is required for yeast growth and normal cell cycle progression. Moreover, a severe truncated allele of Bur1 alone also results in a cell-cycle defect. Together these results indicate that Bur1 is required for cell-cycle progression. Notably, we found that Bur1 cooperates with TORC1 in vacuole-mediated cell cycle progression via phosphorylation of Sch9, a major target of TORC1. Moreover, we found that TORC1 and Bur1 target sites on Sch9 partially overlap, and that each kinase also targets unique Sch9 sites. Importantly, both kinases are required for Sch9 activation. Our findings demonstrate that for the cell-cycle to proceed, there are multiple upstream targeting signals for Sch9 including TORC1 and Bur1.

The discovery of Bur1 as a second regulator of Sch9 supports the hypothesis that Sch9 requires multiple inputs for its full activation; where each input indicates a key cellular status including nutrient availability, cell cycle commitment, and absence of extreme stress in the environment. Another possibility is that Sch9 has distinct downstream targets, and that Sch9 phosphorylation of each target is regulated via distinct upstream signals. Indeed, Sch9 regulates several downstream pathways including the cell cycle, ribosome biogenesis, pH homeostasis, and lifespan (Fabrizio *et al.*, 2001; Pedruzzi *et al.*, 2003; Jorgensen *et al.*, 2004; Kaeberlein *et al.*, 2005).

Bur1 functions in the nucleus as a regulator of transcriptional elongation, which raises the question of the cellular location where Bur1 phosphorylates Sch9. This study suggests that Bur1 functions in nucleus at some stage in the TORC1 pathway. However, the location where Bur1 phosphorylates Sch9 is unclear. Sch9 is mainly localized at cytoplasm, and is concentrated on the vacuole membrane (Urban

et al., 2007), in addition Sch9 functions in the nucleus (Jorgensen *et al.*, 2004), which suggests that Sch9 shuttles between the vacuole and nucleus. In contrast, Bur1 is mainly localized in the nucleus (Huh *et al.*, 2003). In this study we found that a portion of Bur1 localizes in the cytoplasm, and that a C-terminal truncation of Bur1 reduces this cytoplasmic localization (Fig. EV5, A and B). This raises the possibility that Bur1 has a role(s) in the cytoplasm, and may function in vacuole-mediated cell cycle progression, in parallel with TORC1. It is tempting to speculate that Bur1 may phosphorylate Sch9 at the cytoplasm/vacuole and may move to the nucleus for other role(s) in TORC1 activation. However, an alternative possibility is that for vacuole mediated cell cycle progression, Bur1 acts in the nucleus on Sch9 that was first phosphorylated by TORC1 on the vacuole (see model, Fig. 6C).

. Our study also raises the question of the role of the Bur1 C-terminal tail. A previous study suggested that the C-terminus has a role in binding to Rfa1 which is a subunit of heterotrimeric replication protein A (Clausing *et al.*, 2010). In our study, we detected Sch9 and Bur1 association (Fig. EV4A). Interestingly, the C-terminal region is not required for the association with Sch9, but is required for Bur1 kinase activity. The fact that over-expression of the C-terminal region did not affect either yeast growth or in rapamycin sensitivity (Fig. EV4), indicates that the C-terminal region does not impact cell function. Taken together, these results suggest that the C-terminal region works with other region of Bur1 in an intra-molecular manner and is required for Bur1 kinase activity and perhaps Bur1 interaction with other molecules. Notably, the entire C-terminus of Bur1 is composed of a predicted intrinsic disorder region (IDR) (Oates *et al.*, 2013). Sch9 also has predicted IDRs. It has been proposed that IDR can induce liquid-liquid phase separation through multivalent interactions (Shin and Brangwynne, 2017). It is possible that these IDRs are critical for Bur1 activation of Sch9.

It is not clear why the Bur1 C-terminal tail is only essential in vacuole inheritance mutants, *vac17*Δ, *vac8*Δ, and *myo2-N1304*D (Fig. 1H, and Fig. EV1). This may be due to defects in these mutants in TORC1 signaling from an immature vacuole (Jin and Weisman, 2015). In this scenario, wild-type Bur1 may compensate for TORC1. Alternatively, or in addition, the *bur1-ΔC* mutant may retain a low level of kinase activity for Sch9, which is sufficient when vacuole inheritance is normal and cells inherit a mature vacuole. Under these conditions, the levels of Bur1 and/or TORC1 activity required to activate Sch9 may be less. However, the delay in the

maturation of vacuoles in vacuole inheritance mutants likely imposes a severe stress on cells which require enhanced activity of TORC1 and Bur1. Future studies will likely reveal how Bur1 via the vacuole, senses the external and/or internal cellular environment.

Material and methods

Yeast Strain and Media

Yeast strains used are in Table 2. Deletion and fusion strains were constructed as described (Longtine *et al.*, 1998). To generate a *bur1*-Δ*C*::*KanMX* strain, a *Stu*I-*Afe*I fragment from pBlueScript SK+ (pBS) *bur1(1-372)-KanMX* vector was integrated into the *BUR1* locus. To generate a *SCH9-5xHA* strain, a *Not*I cut pRS306 *SCH9-5xHA* plasmid was integrated into *URA3* locus.

Yeast cultures were grown at 24°C unless stated otherwise. Yeast extract-peptone-dextrose (1% yeast extract, 2% peptone, 2% dextrose; YPD), synthetic complete (SC) lacking the appropriate supplement(s), and 5-FOA medium were made as described (Kaiser *et al.*, 1994). Unless stated otherwise, SC medium contained 2% dextrose. For synchronization of yeast at early G1 phase, cells were treated with 9 μM α-mating factor (Peptide Institute, Inc.) for three hours, washed twice, then released to appropriate medium.

***In Vivo* labeling of Vacuoles**

Vacuoles were labeled *in vivo* with N-(3-triethelammoniumpropyl)-4-(6 (4-(diethylamino) phenyl) hexatrienyl) pyridinium dibromide (FM4-64; Molecular Probes) essentially as described (Ishikawa *et al.*, 2003). In brief, a 2 mM stock solution of FM4-64 in dimethyl sulfoxide (DMSO) was added to early log phase cultures for a final concentration of 80 μM. After 1 hr of labeling, cells were washed and then chased in fresh liquid medium for 3-4 hr.

Microscopic analysis

Fluorescence microscopy was performed at room temperature using an inverted fluorescence microscope (IX81; Olympus) equipped with an electron-multiplying CCD camera (ImagEM C9100-13) and a 150× objective lens (UAPON 150× OTIRF, NA/1.45; Olympus), and a confocal microscope (IXplore SpinSR) equipped with an sCMOS camera (ORCA-Flash4.0, Hamamatsu) and a 100x objective lens (UPLAPO 100xOHR, NA/1.50 ; Olympus). Images were acquired and

processed using the MetaMorph software (Molecular Devices), cellSens (Olympus) and Image J (Fiji).

For fluorescent intensity analysis, images were analyzed using CellProfiler software, version 4.1.3 (McQuin *et al.*, 2018). Htb2-mCherry was used as a nuclear marker for unbiased segmentation of cell nuclei and Bur1-mNG was used for cell segmentation using a propagation method. The tertiary cytosolic region was inferred using the two previous segmentations. Integrated intensities were measured for nuclei, cytosol and total cell regions. The ratio of cytosolic/cellular Bur1 intensity was calculated using the CalculateMath module. Statistical analysis and graphing were carried out using GraphPad Prism software version 9.1 using two-tailed unpaired t-tests with a 99% confidence interval.

Plasmids

Plasmids used are in Table 3. To generate YEpGAP yEmRFP-*ADH1*t/*VAC17* plasmid for the color sectoring assay, a *VAC17* fragment cut by *Hind*III and then blunt-ended was inserted at the blunt-ended *Afl*II site of YEpGAP yEmRFP (Keppler-Ross *et al.*, 2008). *ADH1* terminator was amplified by PCR using primers (5'-ATA GGT ACC TGA ACT TCT AAA TAA GCG AAT TTC TTA TG-3') and (5'-TAG TGT ACA TGC CGG TAG AGG TGT GG-3'). *Acc*65I-*Bsr*GI cut fragment of *ADH1* terminator was inserted at *Acc*65I site of YEpGAP yEmRFP/*VAC17* to generate YEpGAP yEmRFP-*ADH1*t/*VAC17*.

For generation of a *BUR1* expression vector, first a 3.8 kb *Acc*65I-*Sal*I fragment of *BUR1* was amplified from yeast genome by PCR using primers (5-ACA gag ctc GGT ACC TGT TTG CAT TTT TGG-3') and (5'-AAT GAA TTC AAA CCT TTA GTC GAC AG-3'). *Sac*I-*Sal*I fragment of *BUR1* was inserted at the *Sac*I and *Sac*II sites of pBS. The *Sac*I-*Sal*I fragment of *BUR1* was subcloned at the *Sac*I and *Sac*II sites of pRS415 or pRS425 for generation of pRS415 *BUR1* or pRS425 *BUR1*, respectively. For generation of YCp50 *BUR1*, an *Zra*I-*Sal*I fragment of *BUR1* from pRS415 *BUR1* was subcloned at the *Nru*I and *Sal*I sites of YCp50 (Rose *et al.*, 1987).

For generation of pBS *bur1*-Δ*C::KanMX*, two *Spe*I sites (after 372 aa position and before stop codon) were inserted into pBS *BUR1* by PCR using primers (5'-GTG ATA TTG CAG ATC TAT Ata cta gtT AGG TTA TAC TAT TCT CTC-3'), (5'-GAG AGA ATA GTA TAA CCT Aac tag tAT ATA GAT CTG CAA TAT CAC-3'), (5'-GTT TAA AGA GGA CCC TTT ACC AaC tag tAA GAT AAC ATT ACC GAC-3'), and (5'-GTC GGT AAT GTT ATC TTa cta GtT GGT AAA GGG TCC

TCT TTA AAC-3'). To generate pBS *bur1*-Δ*C*, a *Spe*I fragment from pBS *BUR1*-SpeI-SpeI were removed by *Spe*I cut, followed by self-ligation. To insert *KanMX* at the 3' region of *BUR1*, *Zra*I site was generated by PCR using primers (5'-CCA TAA AAT CGA AAC TAT TGT CAA gAC GTC AGT ACA TCC TAC CTG-3') and (5'-CAG GTA GGA TGT ACT GAC GTc TTG ACA ATA GTT TCG ATT TTA TGG-3'). The *KanMX* marker was amplified from pFA6a KanMX (Janke et al., 2004) by PCR using primers (5'-GAT TGA CGT CCA GCG ACA TGG AGG CC-3') and (5'-ATG AGA CGT CAC TGG ATG GCG GCG TTA G-3'). *Aat*II fragment of *KanMX* was inserted at the *Zra*I site of 3' region of the *BUR1* to generate pBS *bur1*-Δ*C::KanMX.*

For generation of pRS415 *bur1*-Δ*C*, the *Sac*I-*Sal*I fragment of *bur1*-Δ*C* was subcloned at the *Sac*I and *Sac*II sites of pRS415.

For generation of pRS316 *MYO2*/*BUR1* which has both *MYO2* and *BUR1* genes in a single plasmid, *Nhe*I-*Eco*53kI fragment of *MYO2* from pRS413 *MYO2* was subcloned into pRS316 *BUR1* at *Nhe*I and *Eco*53kI sites to generate pRS316 *MYO2*/*BUR1*.

pRS315 *TOR1* includes 227 bp upstream and 944 bp downstream of the *TOR1* gene, the same region as pRS416 *TOR1* (Jin and Weisman, 2015). pRS415 *TOR2* includes 2,662 bp upstream and 1,642 bp downstream of the *TOR2* gene.

For generation of pVT102-His *BUR2* or pVT102-Ura *BUR2*, the *BUR2* fragment were amplified by PCR using primers (5'-CAG Tgg atc cAT GTC TGC TAC ATC TTC AAG TGG-3') and (5'-TAC Tct gca gTT ATA TTT TAG GTT TTT TGG CAT CTG-3'). *Bam*HI-*Sac*II fragment of *BUR2* were inserted at the *Bam*HI, *Sac*II sites of pVT102-His or pVT102-Ura (Vernet *et al.*, 1987).

For generation of pRS306 *SCH9-5xHA*, *Xho*I-*Not*I fragment of *SCH9-5xHA* from pRS416 *SCH9-5xHA* (Urban *et al.*, 2007) was subcloned at *Xho*I and *Not*I sites of pRS306 (Sikorski and Hieter, 1989). For generation of pRS413 *SCH9* and pRS423 *SCH9*, *Xho*I-*Not*I fragment of *SCH9* from pRS416 *SCH9* (Urban *et al.*, 2007) was subcloned at *Xho*I and *Not*I sites of pRS413 or pRS423 (Sikorski and Hieter, 1989).

For generation of pRS425 *BUR1-5xHA* and pRS425 *bur1*-Δ*C-5xHA*, 5xHA was amplified from pRS416 *SCH9-5xHA* (gift from Dr. Robbie Loewith) by PCR using primers (5'-TTC act agt CCC GGG TTA ATT AAC ATC TTT TAC-3') and (5'-TGG tct aga TTA TGG ATA GGA TCC TGC ATA GTC-3'). *Spe*I-*Xba*I fragment of 5xHA were inserted into *Spe*I site at front of stop codon of *BUR1* or into the *Spe*I site at after

372 aa position of *BUR1* to generate pRS425 *BUR1-5xHA* and pRS425 *bur1-ΔC-5xHA,* respectively.

For generation of alanine substitution of predicted phosphorylation sites of Sch9 mutants, *sch9-9A* (S560A, T568A, T575A, S709A, T710A, S711A, T721A, T723A, and S726A), *sch9-3A* (S709A, T710A, S711A), and *sch9-3D/E* (S709E, T710D, S711E), the *SCH9* gene was mutagenized by site-directed mutagenesis using the following primers: (S560A-S) 5'-TGG TCT TgC TAA AGC TGA CTT GAA GGA TAG-3', (S560A-AS) 5'-GCT TTA GcA AGA CCA AAA TCG CAA AGA GC-3', (T568/T575A-S) 5'-TGA CTT GAA GGA TAG AgC AAA CAC ATT TTG CGG CAC CgC GGA ATA CCT GGC ACC-3', (T568/T575A-AS) 5'-GGT GCC AGG TAT TCC GcG GTG CC CAA AAT GTG TTT GcT CTA TCC TTC AAG TCA-3', (S709/T710/S711A-S) 5'-CCA GAG TTC ACA ACA GCT gCA gCT gCA TAC ATG AAC AAG CAC CAG C-3', (S709/T710/S711A -AS) 5'-GCT GGT GCT TGT TCA TGT ATG cAG cTG cAG CTG TTG TGA ACT CTG G-3', (T721/T723/T726A-S) 5'-GCA CCA GCC GAT GAT GgC TGC TgC CCC GCT AgC TCC AGC CAT GCA AGC-3', (T721/T723/T726A -AS) 5'-GCT TGC ATG GCT GGA GcT AGC GGG GcA GCA GcC ATC ATC GGC TGG TGC-3', (S709E/T710D/S711E-S) 5'-CCA GAG TTC ACA ACA GCT gaA gaT gaA TAC ATG AAC AAG CAC CAG C-3', (S709E/T710D/S711E-AS) 5'-GCT GGT GCT TGT TCA TGT ATt cAt cTt cAG CTG TTG TGA ACT CTG G-3'.

For generation of ADHpRS425 GFP, blunt-ended SphI fragment of *ADH1* promotor from pVT102-Ura vector (Vernet *et al.*, 1987) was subcloned at the blunt-ended *Kpn*I and blunt-ended *Sac*I of pRS425 to generate ADHpRS425. GFP(S65T) was amplified by PCR using primers (5'-AGC ctg cag TAA AGG AGA AGA ACT TTT CAC TGG-3') and (5'-CCA aag ctt TTA ATT AAT ATC CAA ACC AGC TAA TTT CAA AGC TAA TTT GTA TAG TTC ATC CAT GC-3'). The *Pst*I-*Hind*III cut GFP fragment was inserted at *Pst*I and *Hind*III sites of ADHpRS425 to generate ADHpRS425 GFP. *BUR1* and *bur1*-ΔN fragments were amplified by PCR using primers (5'-TAA gga tcc ATG AGT GAT AAT GGT TCC CC-3') (5'-TAG gct agc ATA TAG ATC TGC AAT ATC ACT ATT TTG G-3') and (5'-AAA gga tcc ATG GTT TAC GGG TGT ACA GTT TTC CAG-3'). *Bam*HI-*Sac*I cut *BUR1* or *bur1-ΔN* fragment was inserted at *Bam*HI and *Sac*I sites of ADHpRS425 GFP to generate ADHpRS425 *BUR1-GFP* and ADHpRS425 *bur1-ΔN-GFP*.

For generation of pRS415 *bur1*-Δ*N*, two PCR fragments of *BUR1* were amplified by PCR using primers (5'-AGC ATT TTA CGC TAG CAA TTA TCA ATT TC-3') and (5'-CAC TAG TCA TAT TAT TTT ACT GTT ATT CTG C-3'), and (5'-ATA ATA TGA CTA GTG TTT ACG GGT GTA CAG TTT TCC-3') and (5'-TGA ATA TAA TTT AGG CCT TCT AAT ATT TG-3'). The two PCR fragments were subcloned at *Nhe*I, *Stu*I cut pRS415 *BUR1* by In-Fusion HD cloning Kit (TAKARA BIO INC.).

For addition of mNG, mNG-NLS or mNG-NES to Bur1, mNG fragment was amplified by PCR using primers (5'-TAT act agt ggt cga cgg atc ccc ggg tta att aac GTT TCG AAA GGC GAA GAA GAC AAT GC-3') and (5'-CTA tct aga TTA CTT GTA TAA CTC GTC AGC TCC AAG AAC-3'), (5'-CTA tct aga TTA ATT aac ctt tct ttt ctt ttt tgg CTT GTA TAA CTC GTC AGC TCC AAG AAC-3') or (5'-CTA tct aga TTA ATT AAT ATC CAA ACC AGC TAA TTT CAA AGC TAA CTT GTA TAA CTC GTC AGC TCC AAG AAC-3'). *Spe*I-*Xba*I cut mNG, mNG-NLS or mNG-NES was inserted at *Spe*I site at front of stop codon of *BUR1* to generate pRS416 *BUR1-mNG*, pRS416 *BUR1-mNG-NLS*, pRS416 *bur1*-Δ*N-mNG-NLS*, and pRS426 *BUR1-mNG-NES,* respectively. The *Spe*I-*Xba*I cut mNG-NLS was also inserted at *Spe*I site at after 372 aa position of *BUR1* to generate pRS416 *bur1*-Δ*C-mNG-NLS*.

Flow cytometry analysis

Quantitation of nuclear DNA was determined as follows: Cells were stained with propidium iodide (PI) and analyzed by FACS analysis (BD Accuri™ C6 Flow Cytometer). In most experiments, 40,000 cells were examined. Yeast were in log phase growth. 2.0 OD_{600} yeast cultures were collected, washed with 50 mM of Tris-HCl [pH7.5], and fixed with 70 % EtOH. Cells were then washed twice with 50 mM of Tris-HCl [pH7.5], followed by sonication. Cells were treated with RNaseA (Sigma-Aldrich R6513; final 2 mg/ml in 50 mM of Tris-HCl [pH7.5]) at 37°C for overnight. Cells were then treated with Pepsin (Sigma-Aldrich 7000; final 5 mg/ml) at room temperature for 30 min, and stained with PI (Sigma-Aldrich 4170) 50 mg/ml in 180 mM Tris-HCl [pH7.5], 180 mM NaCl, 70 mM $MgCl_2$) for 1hr at room temperature. The PI stained cells were analyzed by FACS. Data were processed by ModFit LT for Mac 5.0 software (Verity Software House).

Western Blot Analysis

SDS-PAGE and Western blot analysis were performed using standard procedures. Primary and secondary antibodies were used at the following concentrations: rat anti-HA (1:5000; Roche, 3F10), HRP-goat anti-rat IgG (1:5,000; Jackson ImmunoResearch Laboratories), mouse anti-GFP (1:5000; Roche, 11814460001), mouse anti-Pgk1 (1:20,000; Invitrogen), mouse anti-mNG (1:1000; Chromotek, 32F6), HRP-goat anti-mouse IgG (1:5,000; Jackson ImmunoResearch Laboratories). HRP activity was detected using ECL plus (Amersham Bioscience) or using Femtoglow HRP Substrate (Michigan Diagnostics, 21008), and blots were visualized using X-ray film or using FUSION-FX7 (Vilber-Lourmat) imaging system, respectively. Quantification of each band intensity was performed using Fusion© software (Vilber Lourmat).

***In vitro* kinase assay**

In vitro kinase assay was performed as described (Jin *et al.*, 2014). To test phosphorylation of recombinant Sch9 peptides, *bur1Δ* mutant cells expressing *BUR1-5xHA* and *BUR2* were grown to mid-log phase, collected, and lysed in 50 mM Tris-HCl, pH 7.5, 2 mM sodium pyrophosphate, 0.1% SDS, 1% sodium deoxycholate, 1% Triton X-100, 1 mM PMSF, and 1× protein inhibitor cocktail (Sigma-Aldrich) and then centrifuged at 13,000 g for 10 min. The supernatant was incubated with anti-HA antibody and immobilized on protein A Sepharose beads (Sigma-Aldrich). Beads were washed three times with lysis buffer, twice with lysis buffer containing 150 mM NaCl, and then twice with kinase buffer (10 mM Tris-HCl, pH 7.4, 10 mM MgCl2, 50 mM NaCl, 2 mM EDTA, and 1 mM DTT). Beads were incubated with 20–40 µg substrate protein, 2.5 mM ATP, and 0.125 µCi γ-[^{32}P]ATP in kinase buffer at 30°C for 45 min. Reactions were terminated with equal volumes 2× SDS sample buffer.

LC-MS/MS analysis

In vitro kinase assay sample was eluted by Laemmli buffer, followed by SDS-PAGE. The proteins were excised from gel, destained and digested in the gels with 12.5 ng/µl trypsin (Wako) in 50 mM ammonium bicarbonate overnight at 37°C. The peptides were desalted with 3 M Empore C18 Solid Phase Extraction Disks (Sigma). NanoLC-MS/MS analysis was conducted using a Q Exacitve hybrid quadrupole-orbitrap mass spectrometer (Thermo Fisher Scientific), with Xcalibur software, and coupled to an EASY-nLC 1000 (Thermo Fisher Scientific). The data were processed, searched and quantified using Proteome Discoverer (version 2.1.0.81, Thermo Fisher

Scientific), employing the *S. cerevisiae* UniProt database (version Feb. 21, 2016) containing 6749 entries. The search parameters were as follows: trypsin digestion with two missed cleavage permitted; variable modifications, protein N-terminal acetylation, oxidation of methionine, propionamidation of cysteine and phosphorylation of serine, threonine and tyrosine; peptide charge (2+, 3+ and 4+); peptide mass tolerance for MS data, ±10 p.p.m.; and fragment mass tolerance, ±0.02 Da.

Statistical analyses

For all the statistical analyses were performed using GrapPad Prism 9 (GraphPad Software). Statistical significance determined with a one-way ANOVA and Tukey post hoc test.

Acknowledgements

We would like to thank Dr. Robbie Loewith for the pRS416 *SCH9-5xHA* plasmid, Dr. Neta Dean for the YEpGAP yEmRFP plasmid, and Dr. Amir Khan for pGST-Parallel1 plasmid. Drs Hitoshi Nakatogawa, Hiroshi Kimura, and Hiroshi Iwasaki for helping with microscopy and FACS analyses; Drs. Ishihama, Imami and Yachigo for advising and helping with the phospho-proteomic analysis. We thank all members of the Weisman lab and the Ohsumi lab for insightful discussions and suggestions. We thank Emily Kauffman for technical assistance, Steven Merz for helping the EMS mutagenesis screen, and Dr. Alexander May for reading and editing initial draft of the manuscript. The authors thank the Biomaterials Analysis Division, Tokyo Institute of Technology for DNA sequencing analysis. This work was supported by Grant-in-Aid for Research Activity (KAKENHI) 17H06678 and 18K06211 to YJ, and 16H06375 to Y. Ohsumi, and National Institutes of Health (NIH) Grants R01-GM062261 to LSW.

Author contributions: Conceptualization: Y.J. and L.S.W. Data curation: T.E.W. Funding acquisition: Y.J., T.E.W., Y.Oh, and L.S.W. Investigation: Y.J., N.J., and M.K. Methodology: Y.Oi. and R.B. Analysis and interpretation of the data: Y.J., N.J., Y.Oh, and L.S.W. Writing-original draft: Y.J. Writing-review and editing: Y.J., Y.Oh, and L.S.W.

Conflict of interests: The authors declare that they have no competing interests.

Data availability: All data to understand and assess the conclusions of this research are available in the main text and supplementary materials. No data were deposited in a public database.

References

Anand, VC, Daboussi, L, Lorenz, TC, and Payne, GS (2009). Genome-wide analysis of AP-3-dependent protein transport in yeast. Mol Biol Cell 20, 1592–1604.

Birkeland, SR, Jin, N, Ozdemir, AC, Lyons, RH, Weisman, LS, and Wilson, TE (2010). Discovery of mutations in Saccharomyces cerevisiae by pooled linkage analysis and whole-genome sequencing. Genetics 186, 1127–1137.

Bonangelino, CJ, Catlett, NL, and Weisman, LS (1997). Vac7p, a novel vacuolar protein, is required for normal vacuole inheritance and morphology. Mol Cell Biol 17, 6847–6858.

de Bruin, RAM, McDonald, WH, Kalashnikova, TI, Yates, J, and Wittenberg, C (2004). Cln3 activates G1-specific transcription via phosphorylation of the SBF bound repressor Whi5. Cell 117, 887–898.

Catlett, NL, Duex, JE, Tang, F, and Weisman, LS (2000). Two distinct regions in a yeast myosin-V tail domain are required for the movement of different cargoes. J Cell Biol 150, 513–526.

Catlett, NL, and Weisman, LS (1998). The terminal tail region of a yeast myosin-V mediates its attachment to vacuole membranes and sites of polarized growth. Proc Natl Acad Sci U S A 95, 14799–14804.

Clausing, E, Mayer, A, Chanarat, S, Müller, B, Germann, SM, Cramer, P, Lisby, M, and Strässer, K (2010). The transcription elongation factor Bur1-Bur2 interacts with replication protein A and maintains genome stability during replication stress. J Biol Chem 285, 41665–41674.

Costanzo, M et al. (2010). The genetic landscape of a cell. Science 327, 425–431.

Costanzo, M, Nishikawa, JL, Tang, X, Millman, JS, Schub, O, Breitkreuz, K, Dewar, D, Rupes, I, Andrews, B, and Tyers, M (2004). CDK activity antagonizes Whi5, an inhibitor of G1/S transcription in yeast. Cell 117, 899–913.

Eves, PT, Jin, Y, Brunner, M, and Weisman, LS (2012). Overlap of cargo binding sites on myosin V coordinates the inheritance of diverse cargoes. J Cell Biol 198, 69–85.

Fabrizio, P, Pozza, F, Pletcher, SD, Gendron, CM, and Longo, VD (2001). Regulation of longevity and stress resistance by Sch9 in yeast. Science 292, 288–290.

Huh, W-K, Falvo, JV, Gerke, LC, Carroll, AS, Howson, RW, Weissman, JS, and O'Shea, EK (2003). Global analysis of protein localization in budding yeast. Nature 425, 686–691.

Irie, K, Nomoto, S, Miyajima, I, and Matsumoto, K (1991). SGV1 encodes a CDC28/cdc2-related kinase required for a G alpha subunit-mediated adaptive response to pheromone in S. cerevisiae. Cell 65, 785–795.

Ishikawa, K, Catlett, NL, Novak, JL, Tang, F, Nau, JJ, and Weisman, LS (2003). Identification of an organelle-specific myosin V receptor. J Cell Biol 160, 887–897.

Jacinto, E, and Lorberg, A (2008). TOR regulation of AGC kinases in yeast and mammals. Biochem J 410, 19–37.

Jin, N et al. (2014). Roles for PI(3,5)P2 in nutrient sensing through TORC1. Mol Biol Cell 25, 1171–1185.

Jin, N, Jin, Y, and Weisman, LS (2017). Early protection to stress mediated by CDK-dependent PI3,5P2 signaling from the vacuole/lysosome. J Cell Biol 216, 2075–2090.

Jin, Y, Taylor Eves, P, Tang, F, and Weisman, LS (2009). PTC1 is required for vacuole inheritance and promotes the association of the myosin-V vacuole-specific receptor complex. Mol Biol Cell 20, 1312–1323.

Jin, Y, and Weisman, LS (2015). The vacuole/lysosome is required for cell-cycle progression. Elife 4.

Jorgensen, P, Rupes, I, Sharom, JR, Schneper, L, Broach, JR, and Tyers, M (2004). A dynamic transcriptional network communicates growth potential to ribosome synthesis and critical cell size. Genes Dev 18, 2491–2505.

Kaeberlein, M, Powers, RW, Steffen, KK, Westman, EA, Hu, D, Dang, N, Kerr, EO, Kirkland, KT, Fields, S, and Kennedy, BK (2005). Regulation of yeast replicative life span by TOR and Sch9 in response to nutrients. Science 310, 1193–1196.

Kaiser, C, Michaelis, S, and Mitchell, A (1994). Methods in yeast genetics: a Cold Spring Harbor laboratory course manual, Cold Spring Harbor, NY: Cold Spring Harbor Laboratory Press.

Kalderon, D, Roberts, BL, Richardson, WD, and Smith, AE (1984). A short amino acid sequence able to specify nuclear location. Cell 39, 499–509.

Keogh, M-C, Podolny, V, and Buratowski, S (2003). Bur1 kinase is required for efficient transcription elongation by RNA polymerase II. Mol Cell Biol 23, 7005–7018.

Keppler-Ross, S, Noffz, C, and Dean, N (2008). A new purple fluorescent color marker for genetic studies in Saccharomyces cerevisiae and Candida albicans. Genetics 179, 705–710.

Klionsky, DJ, Herman, PK, and Emr, SD (1990). The fungal vacuole: composition, function, and biogenesis. Microbiol Rev 54, 266–292.

Knoblach, B, and Rachubinski, RA (2015). Motors, anchors, and connectors: orchestrators of organelle inheritance. Annu Rev Cell Dev Biol 31, 55–81.

Kosugi, S, Hasebe, M, Tomita, M, and Yanagawa, H (2009). Systematic identification of cell cycle-dependent yeast nucleocytoplasmic shuttling proteins by prediction of composite motifs. Proc Natl Acad Sci U S A 106, 10171–10176.

Liu, Y, Warfield, L, Zhang, C, Luo, J, Allen, J, Lang, WH, Ranish, J, Shokat, KM, and Hahn, S (2009). Phosphorylation of the transcription elongation factor Spt5 by yeast Bur1 kinase stimulates recruitment of the PAF complex. Mol Cell Biol 29, 4852–4863.

Longtine, MS, McKenzie, A, Demarini, DJ, Shah, NG, Wach, A, Brachat, A, Philippsen, P, and Pringle, JR (1998). Additional modules for versatile and

economical PCR-based gene deletion and modification in Saccharomyces cerevisiae. Yeast 14, 953–961.

Lorenz, MC, and Heitman, J (1995). TOR mutations confer rapamycin resistance by preventing interaction with FKBP12-rapamycin. J Biol Chem 270, 27531–27537.

McQuin, C et al. (2018). CellProfiler 3.0: Next-generation image processing for biology. PLoS Biol 16, e2005970.

Moreno-Torres, M, Jaquenoud, M, and De Virgilio, C (2015). TORC1 controls G1-S cell cycle transition in yeast via Mpk1 and the greatwall kinase pathway. Nat Commun 6, 8256.

Murray, S, Udupa, R, Yao, S, Hartzog, G, and Prelich, G (2001). Phosphorylation of the RNA polymerase II carboxy-terminal domain by the Bur1 cyclin-dependent kinase. Mol Cell Biol 21, 4089–4096.

Oates, ME et al. (2013). D^2P^2: database of disordered protein predictions. Nucleic Acids Res 41, D508-516.

Ohsumi, Y (2006). Protein turnover. IUBMB Life 58, 363–369.

Pedruzzi, I, Dubouloz, F, Cameroni, E, Wanke, V, Roosen, J, Winderickx, J, and De Virgilio, C (2003). TOR and PKA signaling pathways converge on the protein kinase Rim15 to control entry into G0. Mol Cell 12, 1607–1613.

Prelich, G, and Winston, F (1993). Mutations that suppress the deletion of an upstream activating sequence in yeast: involvement of a protein kinase and histone H3 in repressing transcription in vivo. Genetics 135, 665–676.

Rose, MD, Novick, P, Thomas, JH, Botstein, D, and Fink, GR (1987). A Saccharomyces cerevisiae genomic plasmid bank based on a centromere-containing shuttle vector. Gene 60, 237–243.

Shaner, NC et al. (2013). A bright monomeric green fluorescent protein derived from Branchiostoma lanceolatum. Nat Methods 10, 407–409.

Shin, Y, and Brangwynne, CP (2017). Liquid phase condensation in cell physiology and disease. Science 357.

Sikorski, RS, and Hieter, P (1989). A system of shuttle vectors and yeast host strains designed for efficient manipulation of DNA in Saccharomyces cerevisiae. Genetics 122, 19–27.

Suzuki, K, Sako, K, Akiyama, K, Isoda, M, Senoo, C, Nakajo, N, and Sagata, N (2015). Identification of non-Ser/Thr-Pro consensus motifs for Cdk1 and their roles in mitotic regulation of C2H2 zinc finger proteins and Ect2. Sci Rep 5, 7929.

Urban, J et al. (2007). Sch9 is a major target of TORC1 in Saccharomyces cerevisiae. Mol Cell 26, 663–674.

Vernet, T, Dignard, D, and Thomas, DY (1987). A family of yeast expression vectors containing the phage f1 intergenic region. Gene 52, 225–233.

Wang, YX, Catlett, NL, and Weisman, LS (1998). Vac8p, a vacuolar protein with armadillo repeats, functions in both vacuole inheritance and protein targeting from the cytoplasm to vacuole. J Cell Biol 140, 1063–1074.

Weisman, LS (2006). Organelles on the move: insights from yeast vacuole inheritance. Nat Rev Mol Cell Biol 7, 243–252.

Wen, W, Meinkoth, JL, Tsien, RY, and Taylor, SS (1995). Identification of a signal for rapid export of proteins from the nucleus. Cell 82, 463–473.

Yao, S, Neiman, A, and Prelich, G (2000). BUR1 and BUR2 encode a divergent cyclin-dependent kinase-cyclin complex important for transcription in vivo. Mol Cell Biol 20, 7080–7087.

Table 1 Sch9 peptide sequences containing Bur1 sites identified by mass spectrometric analysis in this study.

Positions(aa)	Annotated Sequence	Modification	Modified amino acids	# PSMs
684-715	[K].IPPPFKPHLVSETDTSNFDPEFTTA**ST**S**T**SYMNK.[H]	1xPhospho [S/T]	S709, T710, or S711	2
684-715	[K].IPPPFKPHLVSETDTSNFDPEFTTAS**T**SYMNK.[H]	1xPhospho [T27]	T710	1
684-715	[K].KIPPPFKPHLVSETDTSNFDPEFTTAS**T**SYMNK.[H]	1xPhospho [T28]	T710	1
684-715	[K].KIPPPFKPHLVSETDTSNFDPEFTTAS**T**SYMNK.[H]	1xPhospho [T28]	T710	1
538-561	[R].DLKPENILLDANGNIALCDFGL**S**K.[A]	1xPhospho [S23]	S560	1
568-591	[R].**T**NTFCG**TT**EYLAPELLLDETGYTK.[M]	1xPhospho [T]	T568, T574, or T575	8
716-732	[K].HQPMM**T**A**T**PL**S**PAMQAK.[F]	1xPhospho [T/S]	T721, T723, or S726	4
716-732	[K].HQPMMTATPL**S**PAMQAK.[F]	1xPhospho [S11]	S726	3
716-732	[K].HQPMMTATPL**S**PAMQAK.[F]	1xPhospho [S11]	S726	1

Table 2 Yeast strains used in this study

Strain	Genotype	Source	Figure
LWY7235	*MATa, ura3-52, leu2-3,-112, his3-Δ200, trp1-Δ901, lys2-801, suc2-Δ9* (Wild-type)	(Bonangelino *et al.*, 1997)	2,4,EV 3,EV4
YJY988	*MATa/α, VAC17/vac17Δ::TRP1*, *BUR1/bur1-267*	This study	1
YJY679	*MATa/α, VAC17/vac17Δ::hphNT1*, *BUR1/bur1-ΔC::KanMX*	This study	1
LWY17545	*MATa, bur1Δ::KanMX,* YCp50 *BUR1*	This study	1,5,EV 1,EV5
LWY17547	*MATa, bur1Δ::KanMX, vac17Δ::TRP1,* YCp50 *BUR1*	This study	1
YJY684	*MATa* (Wild-type)	This study	2
YJY685	*MATa, bur1-ΔC::KanMX*	This study	2,5,6,EV3,EV 4
YJY680	*MATa, vac17Δ::hphNT1*	This study	2,4
YJY681	*MATa, bur1-ΔC::KanMX, vac17Δ::hphNT1*	This study	2
YJY981	*MATa, bur1-267*	This study	2
YJY977	*MATa, bur1-267, vac17Δ::TRP1*	This study	2

YJY1360	*MATα, WHI5-3xGFP::His3MX, NUP188-mCherry::KanMX, bur1Δ::KanMX*	This study	2
YJY1362	*MATα, WHI5-3xGFP::His3MX, NUP188-mCherry::KanMX, bur1Δ::KanMX, vac17Δ::hphNT1*	This study	2
LWY11678	*MATa, VPH1-GFP::KanMX*	(Jin and Weisman, 2015)	3
YJY691	*MATa, VPH1-GFP::KanMX , vac17Δ:: hphNT1*	This study	3
YJY692	*MATa, VPH1-GFP::KanMX , bur1-ΔC::KanMX*	This study	3
YJY695	*MATa, VPH1-GFP::KanMX , bur1-ΔC::KanMX, vac17Δ::hphNT1*	This study	3
YJY1041	*MATa, ura3-52::SCH9-5xHA::URA3*	This study	4,EV3
YJY1042	*MATa, ura3-52::SCH9-5xHA::URA3, vac17Δ::TRP1*	This study	4,EV3
YJY1045	*MATa, ura3-52::SCH9-5xHA::URA3, bur1-267*	This study	4,EV3
YJY1044	*MATa, ura3-52::SCH9-5xHA::URA3, bur1-267, vac17Δ::TRP1*	This study	4,EV3
YJY895	*MATa, ura3-52::SCH9-5xHA::URA3, bur1-ΔC::KanMX*	This study	4,EV3
YJY897	*MATa, ura3-52::SCH9-5xHA::URA3, bur1-ΔC::KanMX, vac17Δ::hphNT1*	This study	4,EV3
LWY9611	*MATa, tor1Δ::KanMX*	(Jin *et al.*, 2014)	4,5,EV 3
YJY1239	*MATa, tor1Δ::KanMX, bur1-ΔC::KanMX*	This study	4,EV3
LWY18401	*MATa, bur1Δ::KanMX, vac8Δ::HIS3,* YCp50 *BUR1*	This study	EV1
LWY17297	*MATa, bur1Δ::KanMX, myo2Δ::TRP1,* pRS316 *MYO2/BUR1*	This study	EV1
LWY15799	*MATa, WHI5-3xGFP::His3MX*	(Jin and Weisman, 2015)	EV2
LWY15791	*MATa, WHI5-3xGFP::His3MX, vac17Δ::TRP1*	(Jin and Weisman, 2015)	EV2
YJY1036	*MATa, WHI5-3xGFP::His3MX, bur1-267*	This study	EV2

YJY1035	*MATa, WHI5-3xGFP::His3MX, bur1-267, vac17Δ::TRP1*	This study	EV2
YJY601	*MATa, bur1Δ::KanMX, vac17Δ::hphNT1,* YCp50 *BUR1*	This study	EV3,EV4,EV5
LWY13946	*MATα, vac17Δ::TRP1, tor1Δ::KanMX,* pRS416 *VAC17*	This study	EV3
LWY14347	*MATa, sch9Δ::KanMX,* pRS416 *SCH9*	This study	EV4
LWY14348	*MATa, sch9Δ::KanMX, vac17Δ::TRP1,* pRS416 *SCH9*	This study	EV4
YJY1308	*MATa, BUR1-mNG::natNT2, HTB2-mCherry::KanMX*	This study	EV5
YJY1313	*MATa, bur1-ΔC-mNG::natNT2, HTB2-mCherry::KanMX*	This study	EV5

Each above haploid strain is *ura3-52, leu2-3,-112, his3-Δ200, trp1-Δ901, lys2-801, suc2-Δ9*, and diploid strain is *ura3-52/ura3-52, leu2-3,-112/leu2-3,-112, his3-Δ200/his3-Δ200, trp1-Δ901/trp1-Δ901, lys2-801/lys2-801, suc2-Δ9/suc2-Δ9*.

Table 3 Plasmids used in this study

Plasmid name	Description	Source	Figure
YEpGAP yEmRFP-*ADH1*t/*VAC17*	2μ, *URA3*	This study	1
YCp50 *BUR1*	CEN, *URA3*	This study	1,2,5,EV1,EV3,EV4,EV5
pRS415	CEN, *LEU2*	(Sikorski and Hieter, 1989)	1,EV1,EV5
pRS415 *BUR1*	CEN, *LEU2*	This study	1,2,EV1,EV5
pRS415 *bur1-ΔC*	CEN, *LEU2*	This study	1,2,EV1,EV3,EV4,EV5

pRS306 *SCH9-5xHA*	*URA3*	This study	4,EV3
pBS *bur1-ΔC-KanMX*	Amp	This study	1
pVT102-U	2µ, *URA3*	(Vernet et al., 1987)	5
pVT102-U *SCH9*	2µ, *URA3*	This study	5
pVT102-U *sch9-2D3E*	2µ, *URA3*	This study	5
pVT102-U *sch9-3A-2D3E*	2µ, *URA3*	This study	5
pVT102-U *sch9-3D/E*	2µ, *URA3*	This study	5
pVT102-U *sch9-3D/E-2D3E*	2µ, *URA3*	This study	5
pRS426	2µ, *URA3*	(Sikorski and Hieter, 1989)	5,6,EV 3,EV4
pRS426 *TOR1*	2µ, *URA3*	This study	5,EV3
pRS426 *BUR1*	2µ, *URA3*	This study	6,EV3, EV4
pRS425 *BUR1-5xHA*	2µ, *LEU2*	This study	5,EV4
pRS425 *bur1-ΔC-5xHA*	2µ, *LEU2*	This study	5,EV4
pVT102-U *BUR2*	2µ, *URA3*	This study	5,EV4
pGST-Parallel1	Amp	from Dr Amir Khan	5
pGST-Parallel1 Sch9-N (1-390)	Amp	(Jin *et al.*, 2014)	5
pGST-Parallel1 Sch9-C (390-end)	Amp	(Jin *et al.*, 2014)	5
pRS416	CEN, *URA3*	(Sikorski and Hieter, 1989)	6
pRS416 *BUR1*	CEN, *URA3*	This study	6
pRS416 *BUR1-mNG*	CEN, *URA3*	This study	6
pRS416 *BUR1-mNG-NLS*	CEN, *URA3*	This study	6
pRS416 *bur1-ΔC*	CEN, *URA3*	This study	6
pRS416 *bur1-ΔC-mNG-NLS*	CEN, *URA3*	This study	6
pRS416 *bur1-ΔN*	CEN, *URA3*	This study	6

pRS426 *bur1-ΔN*	2μ, *URA3*	This study	6
pRS426 *BUR1-mNG*	2μ, *URA3*	This study	6
pRS426 *BUR1-mNG-NES*	2μ, *URA3*	This study	6
pRS426 *bur1-ΔN-mNG-NES`*	2μ, *URA3*	This study	6
pRS413	CEN, *HIS3*	(Sikorski and Hieter, 1989)	EV1,EV4
pRS316 *MYO2/BUR1*	CEN, *URA3*	This study	EV1
pRS413 *MYO2*	CEN, *HIS3*	(Catlett and Weisman, 1998)	EV1
pRS413 *myo2-N1304D*	CEN, *HIS3*	(Catlett *et al.*, 2000)	EV1
pRS413 *VAC17*	CEN, *HIS3*	(Jin and Weisman, 2015)	EV3,EV4
pRS423	2μ, *HIS3*	(Sikorski and Hieter, 1989)	EV3
pRS423 *TOR1*	2μ, *HIS3*	This study	EV3
pRS415 *VAC17*	CEN, *LEU2*	(Jin *et al.*, 2009)	EV3
pRS315 *TOR1*	CEN, *LEU2*	This study	EV3
pRS415 *TOR2*	CEN, *LEU2*	This study	EV3
pRS425	2μ, *LEU2*	(Sikorski and Hieter, 1989)	EV3
pRS425 *BUR1*	2μ, *LEU2*	This study	EV3
pRS425 *bur1-ΔC*	2μ, *LEU2*	This study	EV3
pVT102-H *BUR2*	2μ, *HIS3*	This study	EV3
pRS426 *BUR1-Venus*	2μ, *URA3*	This study	EV4
pRS426 *bur1(358-end)-Venus*	2μ, *URA3*	This study	EV4
pRS416 *SCH9*	CEN, *URA3*	(Urban *et al.*, 2007)	EV4
pRS413 *SCH9*	CEN, *HIS3*	This study	EV4

pRS413 *sch9-9A* (S560A, T568A, T575A, S709A, T710A, S711A, T721A, T723A, and S726A)	CEN, *HIS3*	This study	EV4
pRS413 *sch9-3A* (S709A, T710A, S711A)	CEN, *HIS3*	This study	EV4
pRS413 *sch9-3D/E* (S709E, T710D, S711E)	CEN, *HIS3*	This study	EV4
pVT102-H	2μ, *HIS3*	(Vernet et al., 1987)	EV4
pVT102-H *SCH9*	2μ, *HIS3*	(Jin and Weisman, 2015)	EV4
pVT102-H *sch9-2D3E*	2μ, *HIS3*	(Jin and Weisman, 2015)	EV4
pVT102-H *sch9-3D/E*	2μ, *HIS3*	This study	EV4
ADHpRS425 *BUR1-GFP*	2μ, *LEU2*	This study	EV5
ADHpRS425 *bur1-ΔN-GFP*	2μ, *LEU2*	This study	EV5
pRS415 *bur1-ΔN*	CEN, *LEU2*	This study	EV5

Figure legends

Figure 1. Mutation of *BUR1* combined with mutations in vacuole inheritance exhibit synthetic growth defects.

(A) Schematic of the synthetic lethal screen used in this study. EMS treated *vac17*Δ cells which have a plasmid expressing yEmRFP and *VAC17*, exhibit a red color colony due to over-expression of the yEmRFP protein. Colonies that retain the red color are likely those that cannot lose the plasmid on non-selective medium, and therefore indicate candidate mutations which are synthetically lethal with the *vac17*Δ mutant.

(B) Schematic of Bur1 protein. Gray box indicates the kinase domain. Blue shaded box; C-terminal tail which is deleted in Bur1-ΔC. Arrow; mutation site of *bur1-267*.

(C) Amino acid alignment by Clustal omega of several CDK kinases in budding yeast. The C-terminal region of Bur1, amino acid residues 373-657 (blue), comprises

an unconventional long tail. This region was deleted in the Bur1-ΔC mutant used in this study. In addition, this region along with several additional amino acids is missing in the *bur1-267* mutant obtained in this study, where W267 (red residue) is substituted with a stop codon. Asterisk; fully conserved residues, colon; strong similarity in amino acid properties, period; weak similarity.

(D) The *bur1-267* mutant exhibits a synthetic growth defect with *vac17Δ*. Haploid colonies from tetrads derived from heterozygous diploids of *VAC17/vac17Δ BUR1/bur1-267* were arrayed vertically on YPD (rich medium) plates incubated at 24 ℃ for 3 days. *vac17Δ = 17Δ*; *bur1-267 = b1*; *bur1-267 vac17Δ* double mutant = *b1,Δ* are indicated.

(E) Quantification of colony size in tetrad dissection, relative to the average of WT colonies. A total of 32 full tetrads were analyzed. Statistical significance (p-value) determined with a one-way ANOVA and Tukey post hoc test. Not a significant difference; ns, p-value > 0.10. **** (p-value < 1 x 10^{-4}). Red bar; average in each category. Error bar; standard deviation (SD).

(F, G) The *bur1-ΔC* mutant exhibits a synthetic growth defect with *vac17Δ*. Quantification of colony size in tetrad dissection, relative to the average of WT colonies. A total of 25 full tetrads were analyzed. p-value determined with a one-way ANOVA and Tukey post hoc test. ** (p-value < 1 x 10^{-2}), *** (p-value < 1 x 10^{-3}). Red bar; average in each category. Error bar; standard deviation (SD).

(H) The *bur1-ΔC* mutant exhibits a synthetic growth defect with the *vac17Δ* mutant. Plasmids were transformed into a *bur1Δ* or *bur1Δ vac17Δ* mutant containing YCp50 [*URA3*] *BUR1*. Plasmids tested were pRS415 [*LEU2*] (mock), pRS415 *BUR1*, or pRS415 *bur1-ΔC*. Transformed colonies were cultured in liquid medium and serial dilutions spotted onto SC+5-FOA or SC-Leu-Ura plates. Plates were incubated at 24 ℃ for 3 days.

Figure 2. A double mutation of *BUR1*/CDK with a vacuole inheritance mutant or a *bur1-267* mutant alone, exhibits a cell cycle delay at G_1 phase.

(A, B) The *bur1-ΔC vac17Δ* double mutant exhibits a delay in progression through G_1 phase of the cell cycle. Yeast were grown in YPD medium and collected in log phase growth. DNA content was measured using propidium iodide (PI) staining and assessed by flow cytometry. p-value determined with a one-way ANOVA and Tukey

post hoc test. ** (p-value < 1 x 10^{-2}). Error bars; SD calculated from at least four independent experiments with at least 100 cells counted in each strain/experiment.

(C, D) A *bur1-267* mutant also exhibits a delay in progression through G_1 phase of the cell cycle. DNA content was measured using PI staining and assessed by flow cytometry. p-value determined with a one-way ANOVA and Tukey post hoc test. **** (p-value < 1 x 10^{-4}). Error bars; SD calculated from at least four independent experiments with at least 100 cells counted in each strain/experiment.

(E, F) The *bur1-ΔC vac17Δ* double mutant shows accumulation of Whi5 in the nucleus. WT, *vac17Δ*, *bur1-ΔC*, and *bur1-ΔC vac17Δ* cells, which express Whi5-3xGFP and Nup188-mCherry from endogenous loci, were incubated at 24℃. Cells were scored for the presence of Whi5-3xGFP in within the nucleus (Nup188-mCherry). Error bars; SD calculated from at least four independent experiments with at least 100 cells counted in each strain/experiment. p-value determined with a one-way ANOVA and Tukey post hoc test. ** (p-value < 1 x 10^{-2}). Error bars; SD calculated from at least four independent experiments with at least 100 cells counted in each strain/experiment. Scale bar, 2 μm.

Figure 3. The double mutation of *BUR1*/CDK with a vacuole inheritance mutant is not defective in *de novo* synthesis of the vacuole

(A) The *bur1*-Δ*C* mutant, but not *bur1*-Δ*C vac17*Δ double mutant, shows normal vacuole inheritance. Quantitative analysis of vacuole inheritance in wild-type, *vac17*Δ, *bur1*-Δ*C, and bur1*-Δ*C vac17*Δ cells. Cells were pulse-chase labeled with FM4-64, and vacuole inheritance was assessed as the percent cells with inherited vacuoles. Error bars; SD calculated from three independent experiments with at least 100 cells counted in each strain/experiment.

(B) The *bur1*-Δ*C vac17*Δ double mutant cells have the ability to generate a vacuole *de novo*, which suggests that the cell-cycle delay is due to a defect in Bur1-dependent signaling. WT, *vac17Δ, bur1*-Δ*C, and bur1*-Δ*C vac17*Δ cells which express Vph1-GFP from its endogenous locus, were pulse labeled with the vacuole specific dye FM4-64. WT and *bur1*-Δ*C* cells have both FM4-64 and Vph1-GFP signals in both mother and daughter cells. *vac17Δ* and *bur1*-Δ*C vac17*Δ cells have both Vph1-GFP and FM4-64 on the vacuole in mother cells, however the daughter cells solely have a Vph1-GFP labeled vacuole, indicating that the vacuole was generated *de novo*, rather

Commented [BA1]: Please define the statistical test. Please define the bars and error bars, e.g. mean ± SD.

Commented [BA2]: Please define the statistical test.

than inherited from the mother vacuole. Arrowheads; new vacuoles in daughter cells. Scale bar, 2 μm.

Figure 4. *BUR1* functions in parallel with the TORC1 pathway.

(A) *In vivo* phosphorylation of Sch9 is reduced in *bur1*-Δ*C vac17*Δ cells. WT, *bur1*-Δ*C*, *vac17*Δ, or *bur1*-Δ*C vac17*Δ *c*ells expressing *SCH9-HA* from the *URA3* locus were grown in YPD. Cell lysates were analyzed by immunoblot with antibodies directed against HA (top) and Pgk1 (loading control).

(B) *In vivo* phosphorylation of Sch9 is reduced in *bur1-267* cells. WT, *vac17*Δ, *bur1-267*, or *bur1-267 vac17*Δ *c*ells expressing *SCH9-HA* from the *URA3* locus were grown in YPD. Cell lysates were analyzed by immunoblot with antibodies directed against HA (top) and Pgk1 (loading control).

(C) *bur1*-Δ*C* shows high rapamycin sensitivity. WT, *tor1*Δ, *bur1*-ΔC, *tor1*Δ *bur1*-ΔC or *vac17*Δ cells were cultured in liquid YPD medium and serial dilutions were spotted onto YPD plates with 0, 2, 4 or 8 ng/ml of rapamycin added. Plates were incubated at 24℃ for 2 days.

Figure 5. Bur1 phosphorylates Sch9 *in vivo* and *in vitro*.

(A) Western blot analysis of immunoprecipitated Bur1-HA or Bur1-ΔC-HA used in (B).

(B) *In vitro*, Bur1 directly phosphorylates the kinase domain of Sch9 as well as Bur1 itself. pRS425 *BUR1*-HA and pVT102-Ura *BUR2*, the essential cyclin for *BUR1*, were co-expressed in a *bur1Δ* mutant, immunoprecipitated using anti-HA antibody and protein A beads, and then incubated with [γ-^{32}P]ATP and GST, GST-N-Sch9 (1–390) or GST-C-Sch9 (391–824). Proteins were eluted with SDS sample buffer, separated by SDS-PAGE, and transferred to nitrocellulose membranes. Membranes exposed to x-ray film (top) or stained with Ponceau S (bottom). Red arrowhead; phosphorylated GST-C-Sch9. Gray arrowhead; auto-phosphorylated Bur1.

(C) Phosphorylation sites determined by mass spectrometry in Sch9 are indicated (red lettering). Green circle; Pkh target site (T570), blue circles; main TORC1 target sites (T723, S726, T737, S758, and S765).

(D) Sch9-2D3E, but not Sch9-3A-2D3E, partially suppressed the rapamycin sensitivity of *tor1*Δ cells. *tor1*Δ which expresses pRS426 (mock), pRS425 *TOR1*,

pVT102-Ura (mock), pVT102-Ura Sch9, pVT102-Ura Sch9-2D3E, or pVT102-Ura Sch9-3A-2D3E, were cultured in liquid SC-Ura medium and serial dilutions spotted onto SC-Ura plates with 0 or 8 ng/ml of rapamycin added. Plates were incubated at 24 ℃ for 2-3 days.

(E) The Sch9-2D3E mutant did not suppress the rapamycin sensitivity of *bur1*-ΔC cells. *bur1*-ΔC which expresses pRS426 (mock), pRS426 *BUR1*, pVT102-Ura (mock), pVT102-Ura *SCH9*, pVT102-Ura *sch9-2D3E*, pVT102-Ura *sch9-3A-2D3E*, pVT102-Ura *sch9-3D/E*, or pVT102-Ura *sch9-3D/E-2D3E* were cultured in liquid SC-Ura medium and serial dilutions spotted onto SC-Ura plates with 0 or 8 ng/ml of rapamycin added. Plates were incubated at 24℃ for 3 days.

Figure 6. Bur1 function in the nucleus is required for TORC1 signaling.

(A) Bur1 fused SV40-NLS does not rescue the rapamycin sensitivity of *bur1-ΔC* compared to Bur1 without the NLS. *bur1-ΔC* which expresses pRS416 (mock), pRS416 *BUR1*, pRS416 *BUR1-mNG,* pRS416 *BUR1-mNG-NLS,* pRS416 *bur1-ΔC,* pRS416 *bur1-ΔC-mNG-NLS* or pRS416 *bur1-ΔN*, were cultured in liquid SC-Ura medium and serial dilutions spotted onto SC-Ura plates with 0, 4, 8, or 16 ng/ml of rapamycin added. Plates were incubated at 24℃ for 2 days.

(B) Adding nuclear-export signal (NES) of PKI to Bur1 and/or deletion of the importin α-dependent NLS from Bur1 resulted in higher sensitivity to rapamycin compared to Bur1 without this NES. *bur1-ΔC* which expresses pRS426 (mock), pRS426 *BUR1*, pRS426 *bur1-ΔN,* pRS426 *BUR1-mNG*, pRS426 *BUR1-mNG-NES,* or pRS426 *bur1-ΔN-mNG-NES*, were cultured in liquid SC-Ura medium and serial dilutions spotted onto SC-Ura plates with 0, 4, 8, or 16 ng/ml of rapamycin added. Plates were incubated at 24℃ for 2 days.

(C) Model for the roles of Bur1, TORC1 and Sch9 for progression through G_1 phase of the cell-cycle. Bur1 and TORC1 act in parallel to phosphorylate Sch9. We propose that similar to TORC1, Bur1 phosphorylates Sch9 on the vacuole membrane, or alternatively that Sch9 which is phosphorylated by TORC1 on the vacuole, translocates to the nucleus where it is further phosphorylated by Bur1. Then Sch9 acts in parallel with Cdc28/Cdk1-Cln3, in a process that results in the export of Whi5 from the nucleus and cell-cycle progression through early G_1 phase.

Expanded View Figure Legends

Figure EV1. Mutation of *BUR1* combined with mutations in vacuole inheritance exhibit synthetic growth defects.

(A) The *bur1-ΔC* mutant exhibits a synthetic growth defect with a *vac8Δ* mutant. Plasmids were transformed into a *bur1Δ*, or a *bur1Δ vac8Δ* mutant containing YCp50 [*URA3*] *BUR1*. Plasmids tested were pRS415 [*LEU2*] (mock), pRS415 *BUR1*, or pRS415 *bur1-ΔC*. Transformed colonies were cultured in liquid medium and serial dilutions spotted onto SC+5-FOA or SC-Leu-Ura plates. Plates were incubated at 24 ℃ for 3 days.

(B) The *bur1-ΔC* mutant also exhibits a synthetic growth defect with *myo2-N1304D* mutant. Plasmids were transformed into a *bur1Δ myo2Δ* mutant containing YCp50 [*URA3*] *BUR1*/*MYO2*. Plasmids tested were pRS415 [*LEU2*] (mock), pRS415 *BUR1*, or pRS415 *bur1-ΔC*, and pRS413[*HIS3*] (mock), pRS413 *MYO2*, or pRS413 *myo2-N1304D*. Transformed colonies were cultured in liquid medium and serial dilutions spotted onto SC-His-Leu+5-FOA or SC-His-Leu-Ura plates. Plates were incubated at 24℃ for 3 days.

Figure EV2. A truncation mutation of *bur1-267* exhibits a cell cycle delay.

(A, B) Both the *bur1-267* single and *bur1-267 vac17Δ* double mutants show accumulation of Whi5 in the nucleus. WT, *vac17Δ*, *bur1-267*, and *bur1-267 vac17Δ* cells, which express Whi5-3xGFP from its endogenous locus, were incubated at 24℃. Cells were scored for the presence of Whi5-3xGFP in the nucleus. Error bars; SD calculated from four independent experiments with at least 100 cells counted in each strain/experiment. p-value determined with a one-way ANOVA and Tukey post hoc test. *** (p-value < 1 x 10^{-3}), **** (p-value < 1 x 10^{-4}). Scale bar, 2 μm.

Commented [BA3]: Please define the statistical test.

Figure EV3. *BUR1* functions in parallel with the TORC1 pathway.

(A) *In vivo* phosphorylation of Sch9 is reduced in *bur1-ΔC*, *bur1-ΔC vac17Δ*, *bur1-267*, or *bur1-267 vac17Δ* cells. WT, *vac17Δ*, *bur1-ΔC*, *bur1-ΔC vac17Δ*, *bur1-267*, or

*bur1-267 vac17*Δ cells expressing *SCH9-HA* from the *URA3* locus were grown in YPD. (Top panel) Cell lysates were separated in phos-tag containing SDS-PAGE gels, and analyzed by immunoblot with antibodies directed against HA. (Bottom panel) Quantification of the ratio of upper-Sch9 to lower Sch9 on phos-tag gel western blots. Red bar; average in each strain. Error bars; SD calculated from three independent experiments. p-value determined with a one-way ANOVA and Tukey post hoc test. *** (p-value < 1 x 10^{-3}), **** (p-value < 1 x 10^{-4}).

(B) Plasmids were transformed into a *bur1Δ vac17Δ* mutant containing YCp50 [*URA3*] *BUR1*. Plasmids tested were pRS415 [*LEU2*] (mock), pRS415 *BUR1*, or pRS415 *bur1*-Δ*C*, with pRS413 [*HIS3*] (mock), pRS413 *VAC17*, pRS423 [*HIS3*] (2μ), or pRS423 *TOR1*. Transformed colonies were cultured in liquid medium and serial dilutions spotted onto 5-FOA-His-Leu or SC-His-Leu-Ura plates. Plates were incubated at 24℃ for 3 days.

(C) Over-expression of *TOR1* rescued the rapamycin sensitivity of the *bur1*-Δ*C* mutant. Plasmids were transformed into WT, *tor1Δ*, *bur1*-Δ*C* or *tor1*Δ *bur1*-Δ*C* mutant. Plasmids tested were pRS426 [*URA3*] (2μ), pRS426 *TOR1*, pRS426 *BUR1*, or pRS426 *bur1-ΔC*. Transformed colonies were cultured in liquid SC-Ura medium and serial dilutions spotted onto SC-Ura plate with 0, 4, or 8 ng/ml of rapamycin added. Plates were incubated at 24℃ for 2 days.

(D) Low copy or over-expression of *BUR1* did not rescue the growth defect of the *tor1*Δ *vac17*Δ mutant. Plasmids were transformed into a *vac17Δ tor1Δ* mutant containing pRS416 [*URA3*] *VAC17*. Plasmids tested were pRS415 [*LEU2*] (mock), pRS415 *VAC17*, pRS415 *TOR1*, pRS415 *TOR2*, pRS415 *BUR1*, pRS425 [*LEU2*] (2μ), pRS425 *BUR1*, or pRS425 *bur1-ΔC*. Transformed colonies were streaked onto 5-FOA or -Leu-Ura plates. Plates were incubated at 24℃ for 3 days.

(E) Over-expression of *BUR1* and *BUR2* did not rescue the growth defect of the *tor1*Δ *vac17*Δ mutant. Plasmids tested were pRS425 [*LEU2*] (2μ), or pRS425 *BUR1*, with pVT102-His (2μ), or pVT102-His *BUR2*, which encodes the *BUR1* cyclin. pRS315 *TOR1* and pRS413 *VAC17* were used as positive controls.

Figure EV4. The Bur1 phospho-sites on Sch9 are important for normal cell growth.

(A) Bur1 is associated with Sch9. Purified bacterially expressed GST-Sch9 protein pulled down Bur1 from yeast lysates. Proteins pulled down by GST, GST-Sch9 (1-390), GST-Sch9 (391-824), and 8% of input yeast lysate analyzed by immunoblot with anti-HA antibodies (top), or by Coomassie brilliant blue (CBB) (bottom).
(B) Over-expression of Bur1 C-terminal region in wild-type yeast does not affect their sensitivity to rapamycin or their growth on normal synthetic media. Plasmids tested were pRS426 [*URA3*] (mock), pRS426 *BUR1*, pRS426 *BUR1-Venus*, or pRS426 *bur1(358-end)-Venus*. Transformed colonies were cultured in liquid medium and serial dilutions were spotted onto SC-Ura plates with 0, 4, 8 or 16 ng/ml of rapamycin added. Plates were incubated at 24℃ for 2 days.
(C) Over-expression of the Bur1 C-terminal region does not rescue the rapamycin sensitivity of *bur1-ΔC* cells.
(D) Western blot analysis of cells expressing Bur1-Venus or Bur1(358-657)-Venus from CEN or 2μ plasmid. Cell lysates were analyzed by immunoblot with antibodies directed against GFP (top) and Pgk1 (loading control).
(E) An Sch9 mutant that is missing the nine novel Bur1 phosphorylation sites identified in this study is not functional, and an Sch9 mutant which is mutated at only three novel adjacent Bur1 sites identified in this study exhibits a growth defect. Plasmids were transformed into a *sch9Δ vac17Δ* mutant containing pRS416 [*URA3*] *SCH9*. Plasmids tested were pRS413 [*HIS3*] (mock), pRS413 *SCH9*, pRS413 *sch9-9A*, pRS413 *sch9-3A*, or pRS413 *sch9-3D/E*. Transformed colonies were cultured in liquid medium and serial dilutions were spotted onto 5-FOA or SC-His-Ura plates. Plates were incubated at 24℃ for 2 days.
(F) The phospho-mimetic sch9-2D3E mutant as well as sch9-3D/E does not rescue the growth defect of the *bur1-ΔC vac17Δ* mutant. Plasmids tested were pRS415 *bur1-ΔC* with pRS413 (mock), pRS413 *VAC17*, pVT102-H (2μ), pVT102-H *SCH9*, pVT102-H *sch9-2D3E*, or pVT102-H *sch9-3D/E*. Transformed colonies were cultured in liquid medium and serial dilutions were spotted onto 5-FOA-His-Leu, 5-FOA-His or SC-His-Leu-Ura plates, and incubated at 24℃ for 3 days.

Figure EV5. Bur1 is distributed between the nucleus and cytoplasm.

(A) The C-terminal truncation of Bur1 exhibited a reduced cytoplasmic localization. Bur1-mNG or Bur1-ΔC-mNG with histone H2B (Htb2)-mCherry were expressed from their endogenous loci. Scale bar, 2 μm.

(B) Quantification of Bur1-mNG intensity in the cytoplasmic region. Ratios of cytoplasmic/total cellular mNG intensity were calculated for both Bur1 and Bur1-ΔC. Statistical significance (p-value) was determined with student t-test. **** (p-value < 1 x 10^{-4}). Red bar; average in each strain. Error bar; SD calculated from at least 300 cells were measured in each strain.

(C) Western blot analysis of cells expressing Bur1-mNG or Bur1-ΔC-mNG. Cell lysates were analyzed by immunoblot with antibodies directed against mNG (top) and Pgk1 (loading control).

(D) The cytosolic pool of Bur1 exhibits some change during cell-cycle. Wild-type yeast which express Bur1-mNG and histone Htb2-mCherry from endogenous loci, were synchronized using α-mating factor arrest and release. Released cells from the α-factor were imaged every 15 min by microscope. For fluorescent intensity analysis, images were analyzed using CellProfiler software (Top panel). Quantification of Bur1-mNG intensity in the cytoplasmic region. Ratios of nuclear/cytoplasm and cytosolic/cell mNG intensity were calculated for Bur1-mNG. (Bottom panel) Cell-cycle synchronicity was monitored using cell morphology combined with histone Htb2-mCherry fluorescence to assess the location of the nucleus: unbudded cell, bud without nucleus, or cell during nuclear segregation.

(E) Full-length Bur1 localizes in the nucleus while Bur1-ΔN (50-657) mainly localizes in the cytoplasmic region in cells. Scale bar, 2 μm.

(F) Bur1-ΔN supports the viability of the *bur1*Δ and *bur1*Δ *vac17*Δ mutants. Plasmids were transformed into a *bur1Δ* or *bur1Δ vac17Δ* double mutant containing YCp50 [*URA3*] *BUR1*. Plasmids tested were pRS415 [*LEU2*] (mock), pRS415 *BUR1*, pRS415 *bur1-ΔN*, or pRS415 *bur1-ΔC*. Transformed colonies were cultured in liquid medium and serial dilutions spotted onto 5-FOA or SC-Leu-Ura plates. Plates were incubated at 24 ℃ for 3 days.

Commented [BA4]: Please define the annotated p-value(s), e.g. *P < 0.05.

Commented [BA5]: Please define the bars and error bars, e.g. mean ± SD.

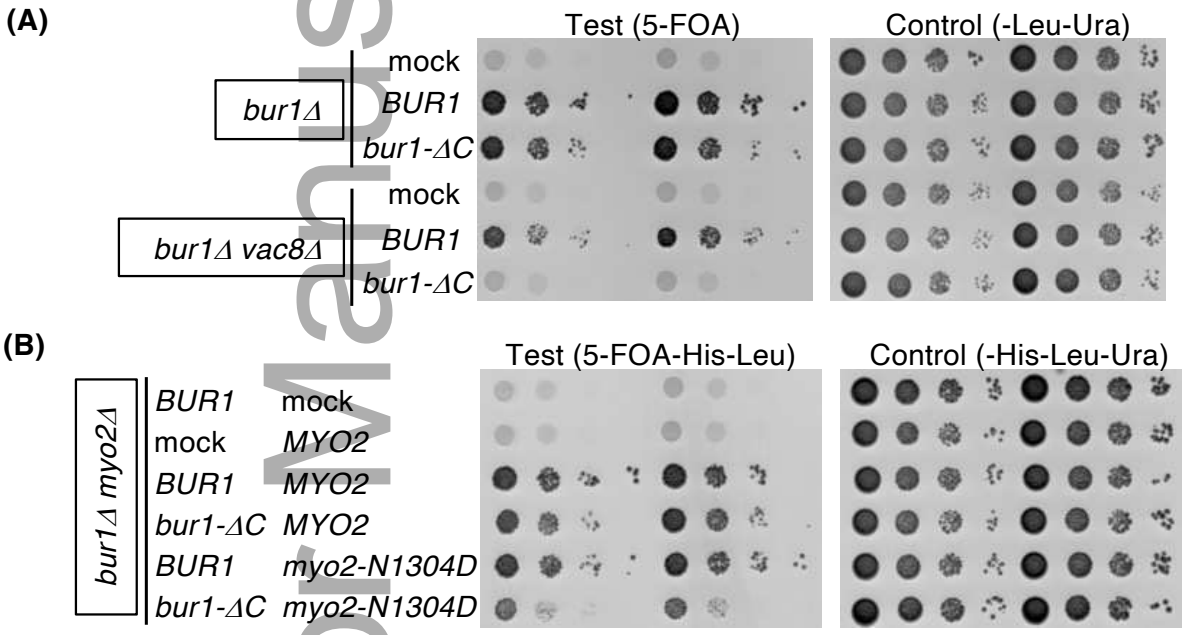

Figure EV1. Mutation of *BUR1* combined with mutations in vacuole inheritance exhibit synthetic growth defects.

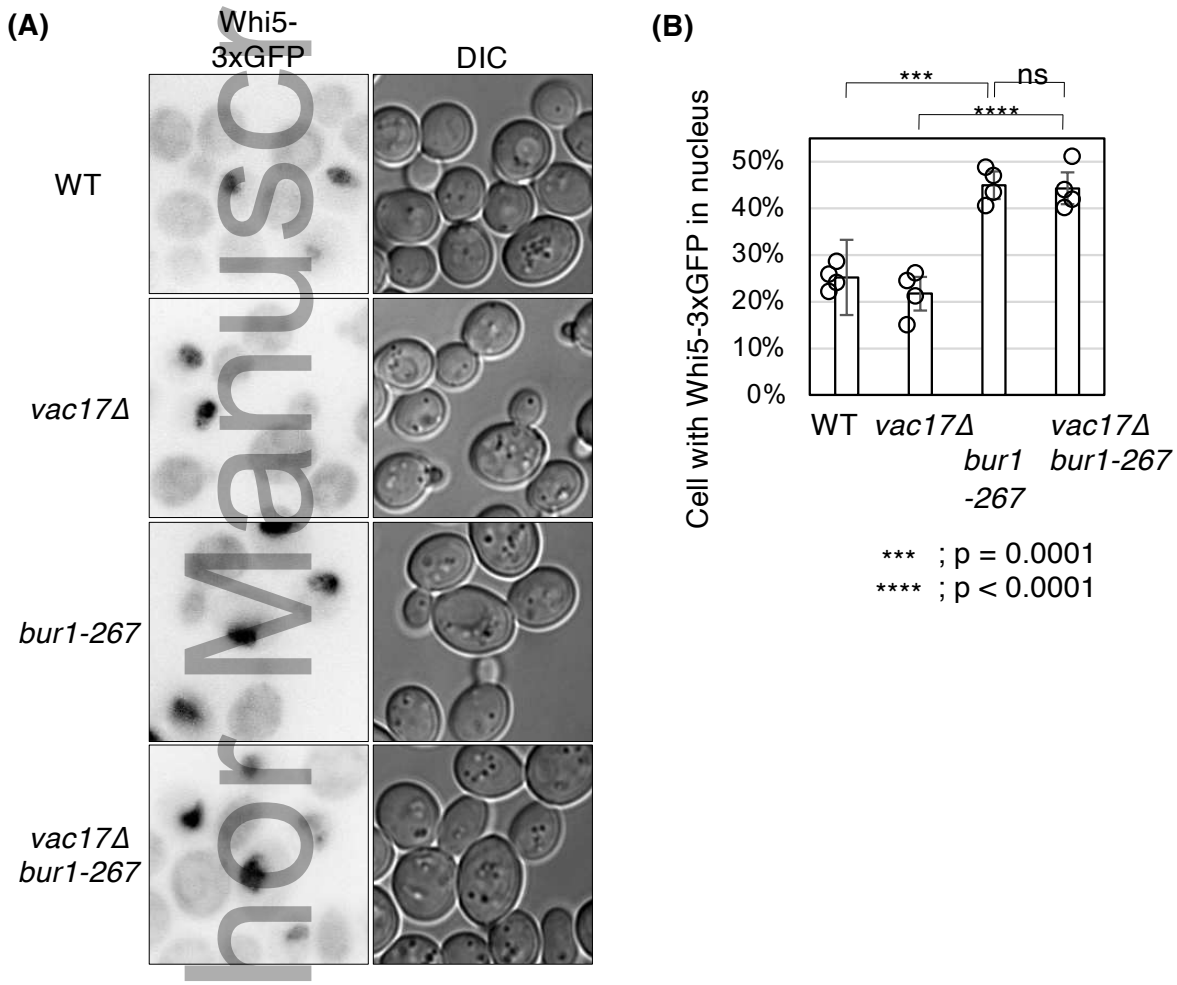

Figure EV2. A truncation mutation of *bur1-267* exhibits a cell cycle delay.

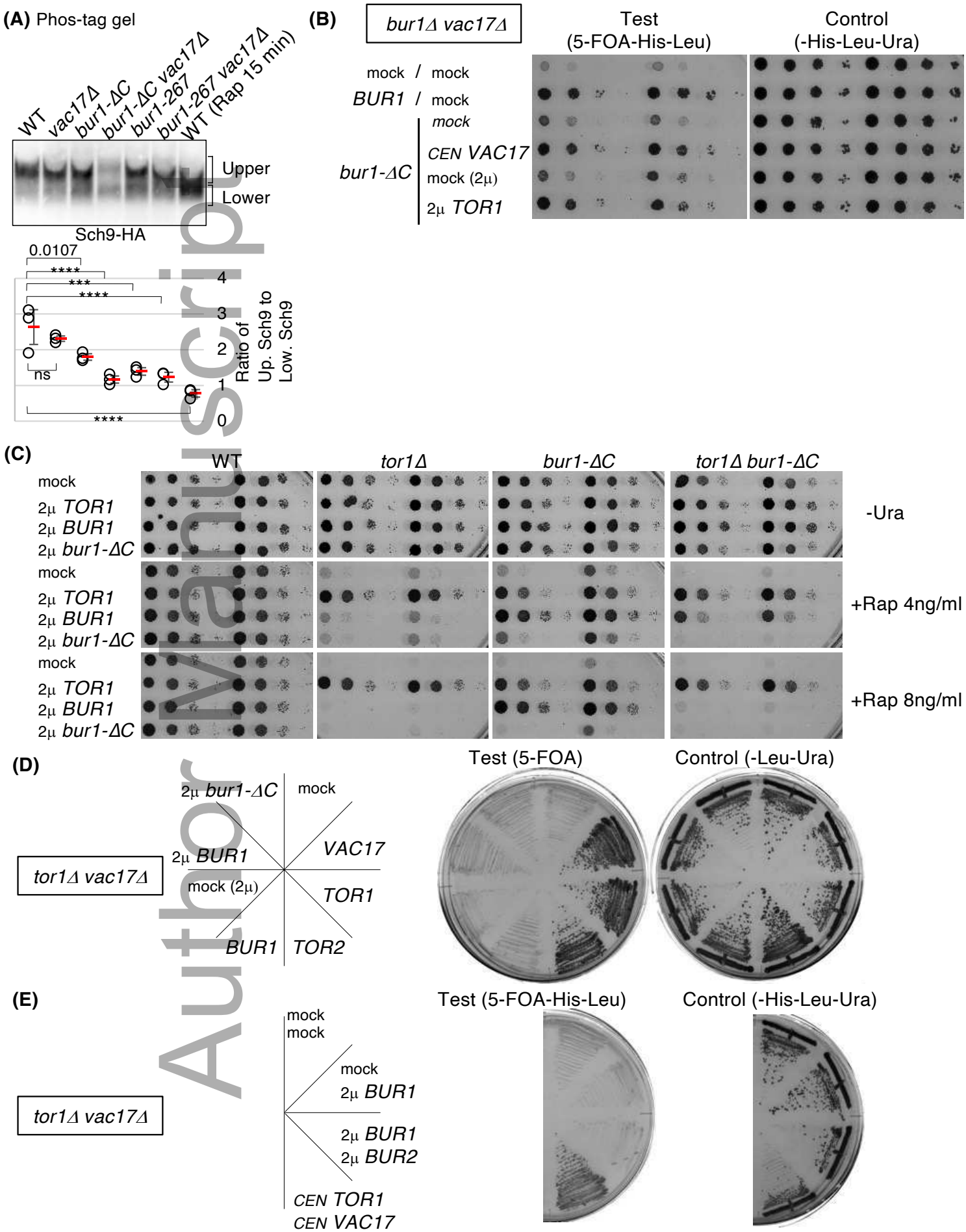

Figure EV3. *BUR1* functions in parallel with the TORC1 pathway.

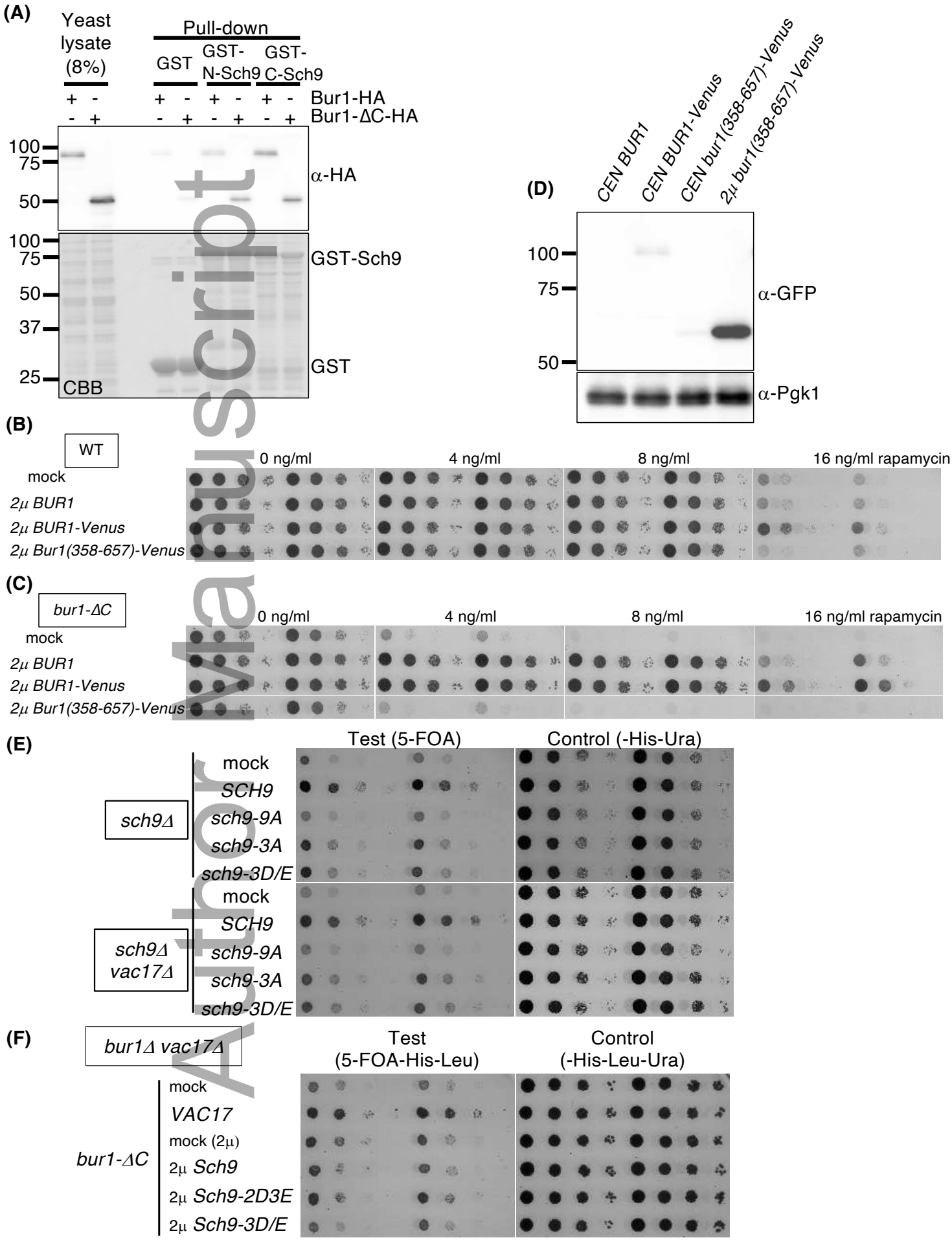

Figure EV4. The Bur1 phospho-sites on Sch9 are important for normal cell growth.

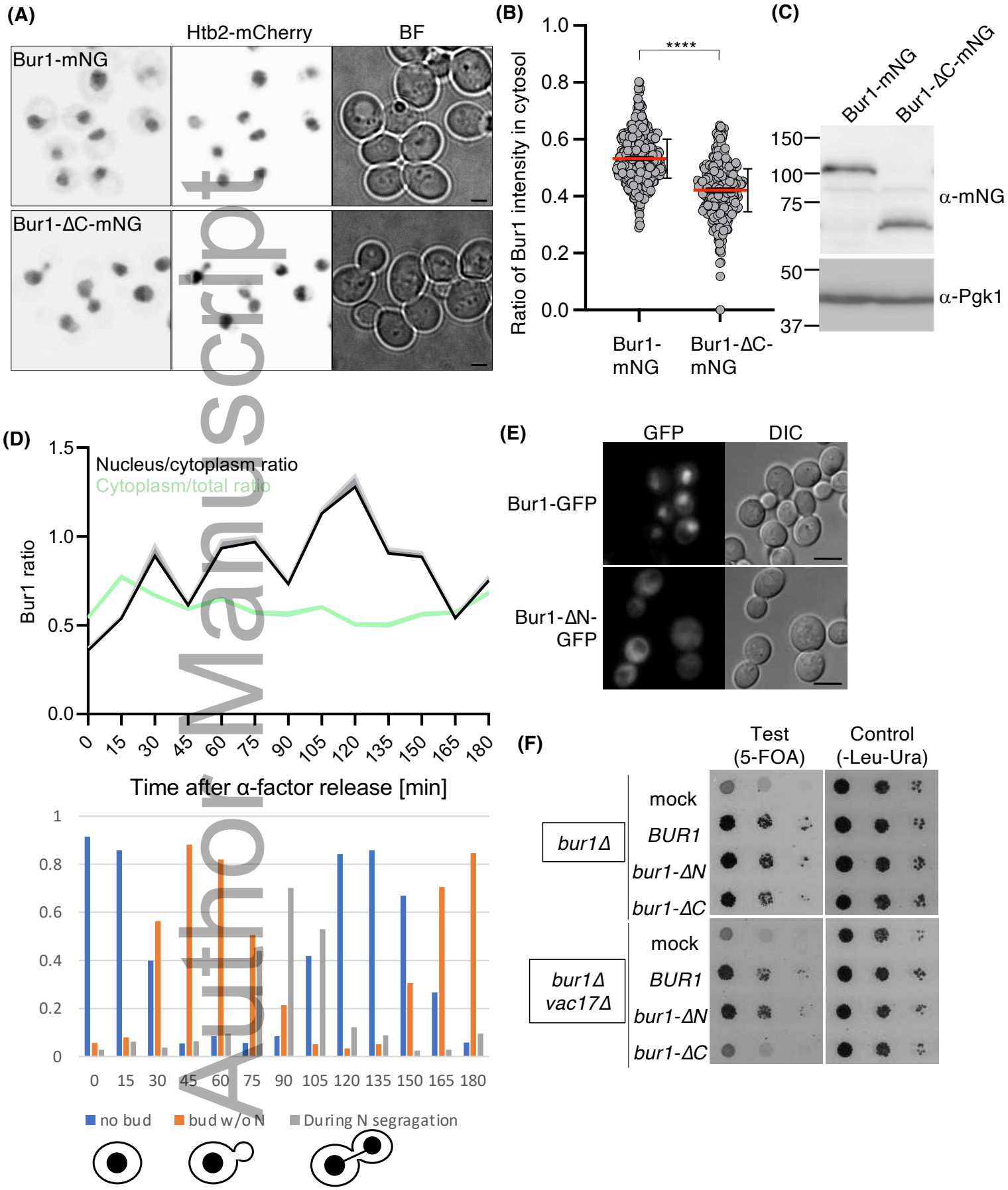

Figure EV5. Bur1 is mostly nuclear with a small portion in the cytoplasm region of the cell.

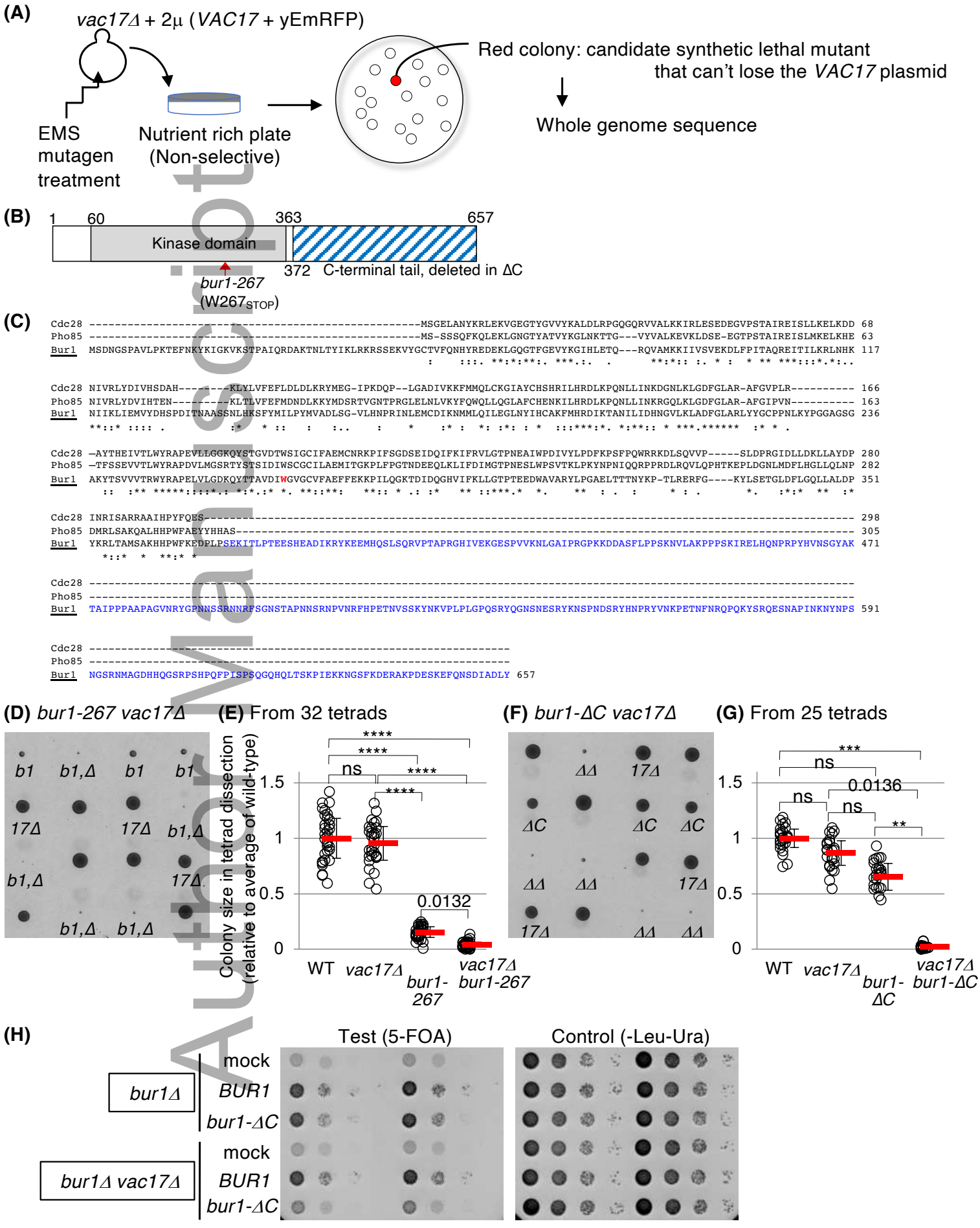

Figure 1. Mutation of *BUR1* combined with mutations in vacuole inheritance exhibit synthetic growth defects.

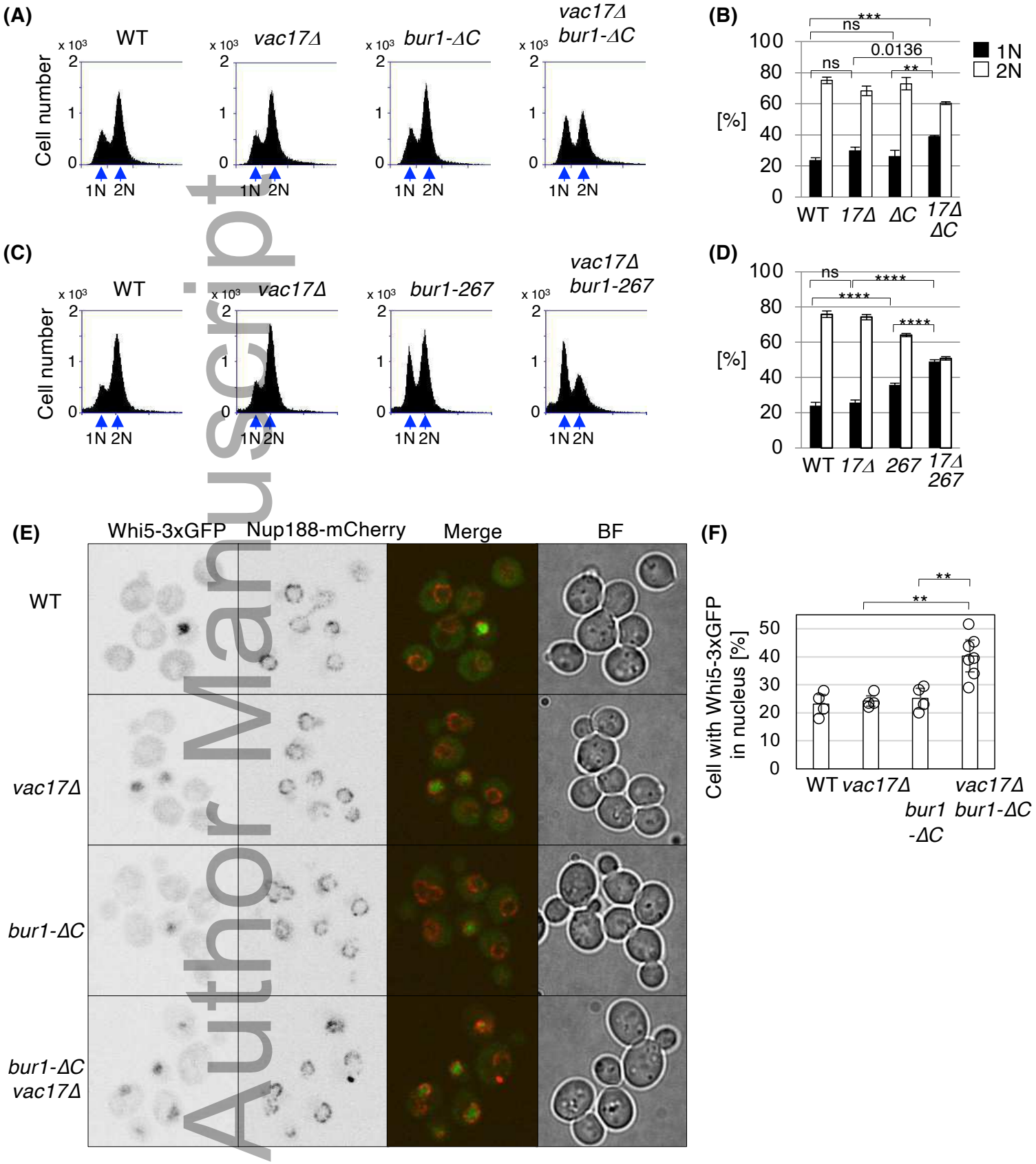

Figure 2. A double mutation of *BUR1*/CDK with a vacuole inheritance mutant or a *bur1-267* mutant alone, exhibits a cell cycle delay at G_1 phase.

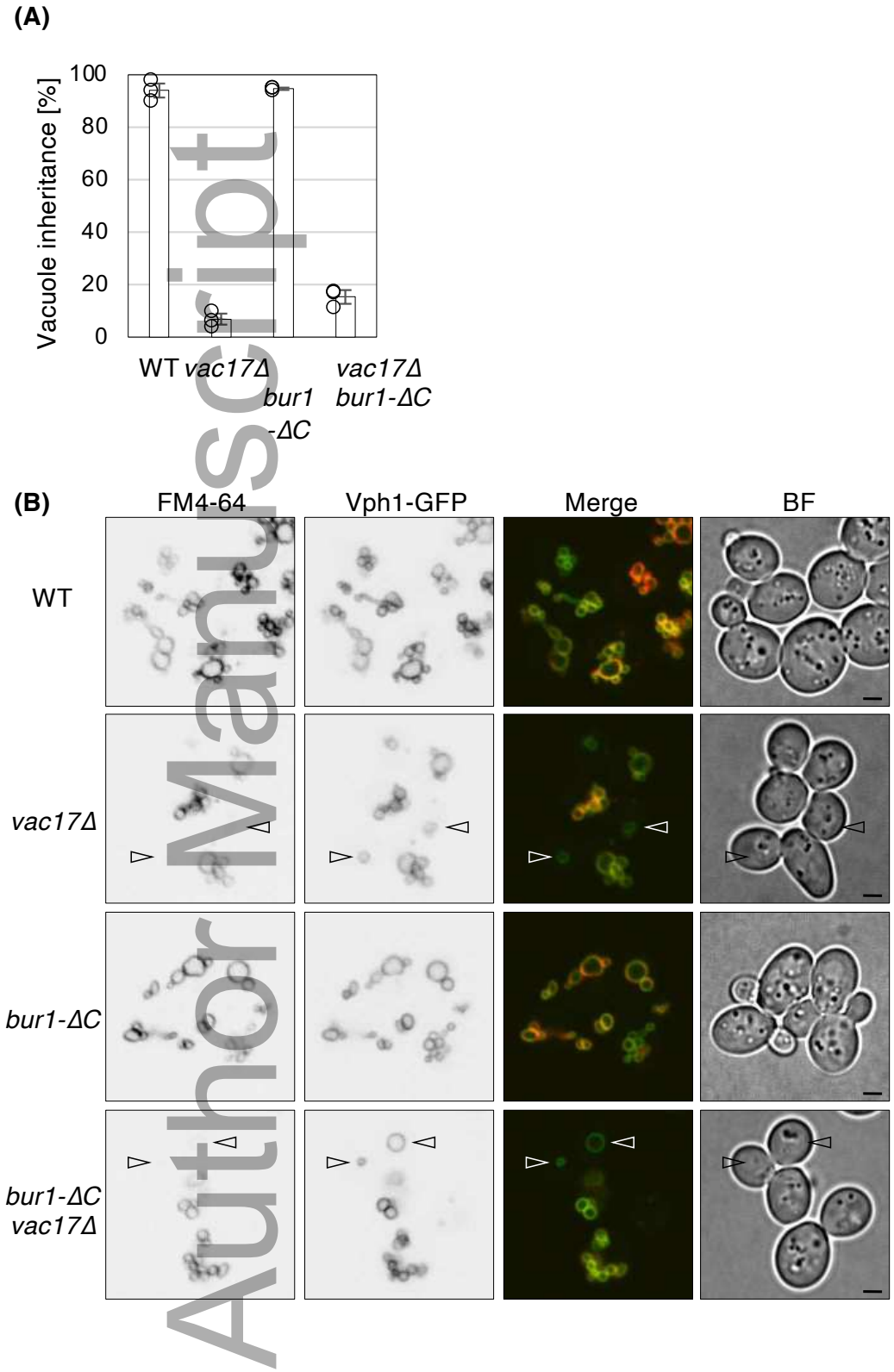

Figure 3. A double mutation of *BUR1*/CDK with a vacuole inheritance mutant is not defective in *de novo* synthesis of the vacuole.

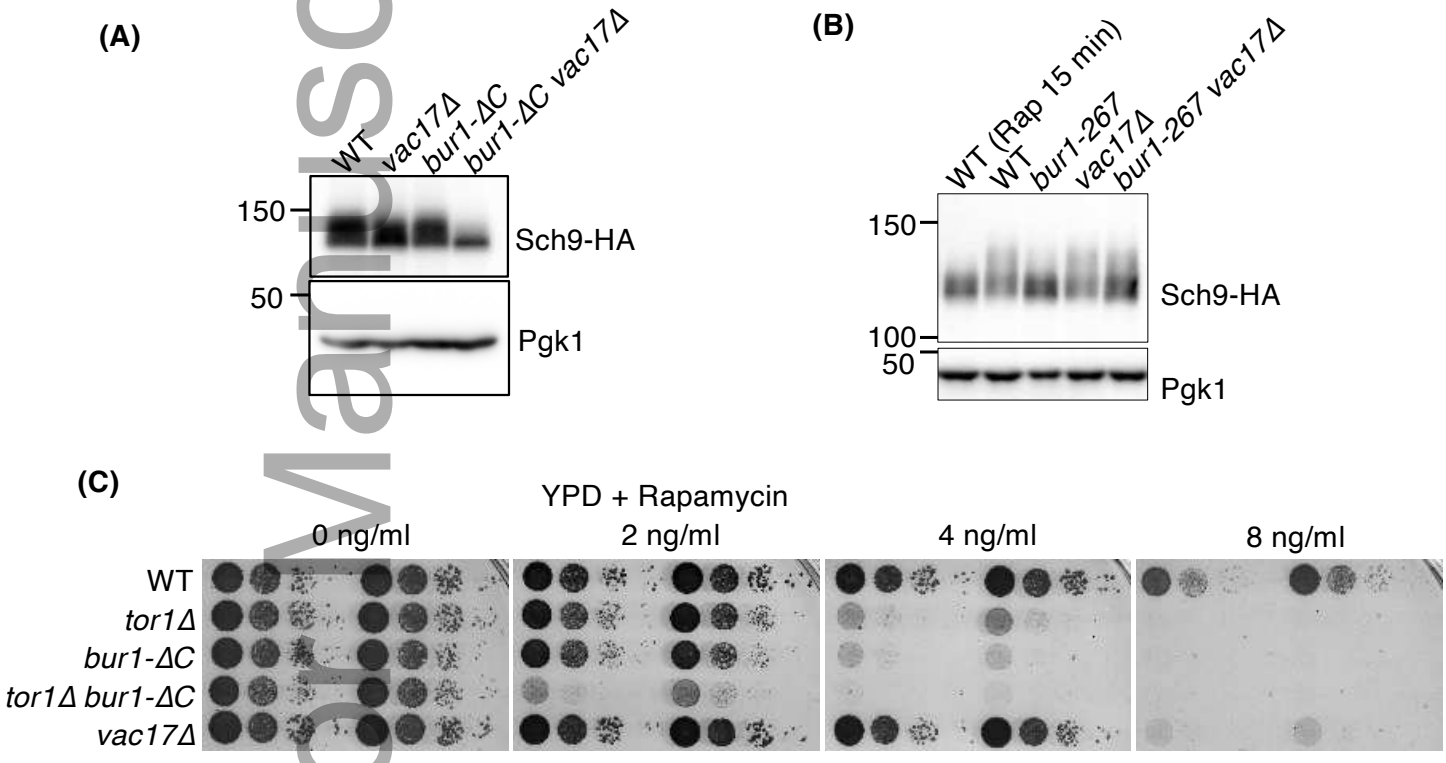

Figure 4. *BUR1* functions in parallel with the TORC1 pathway.

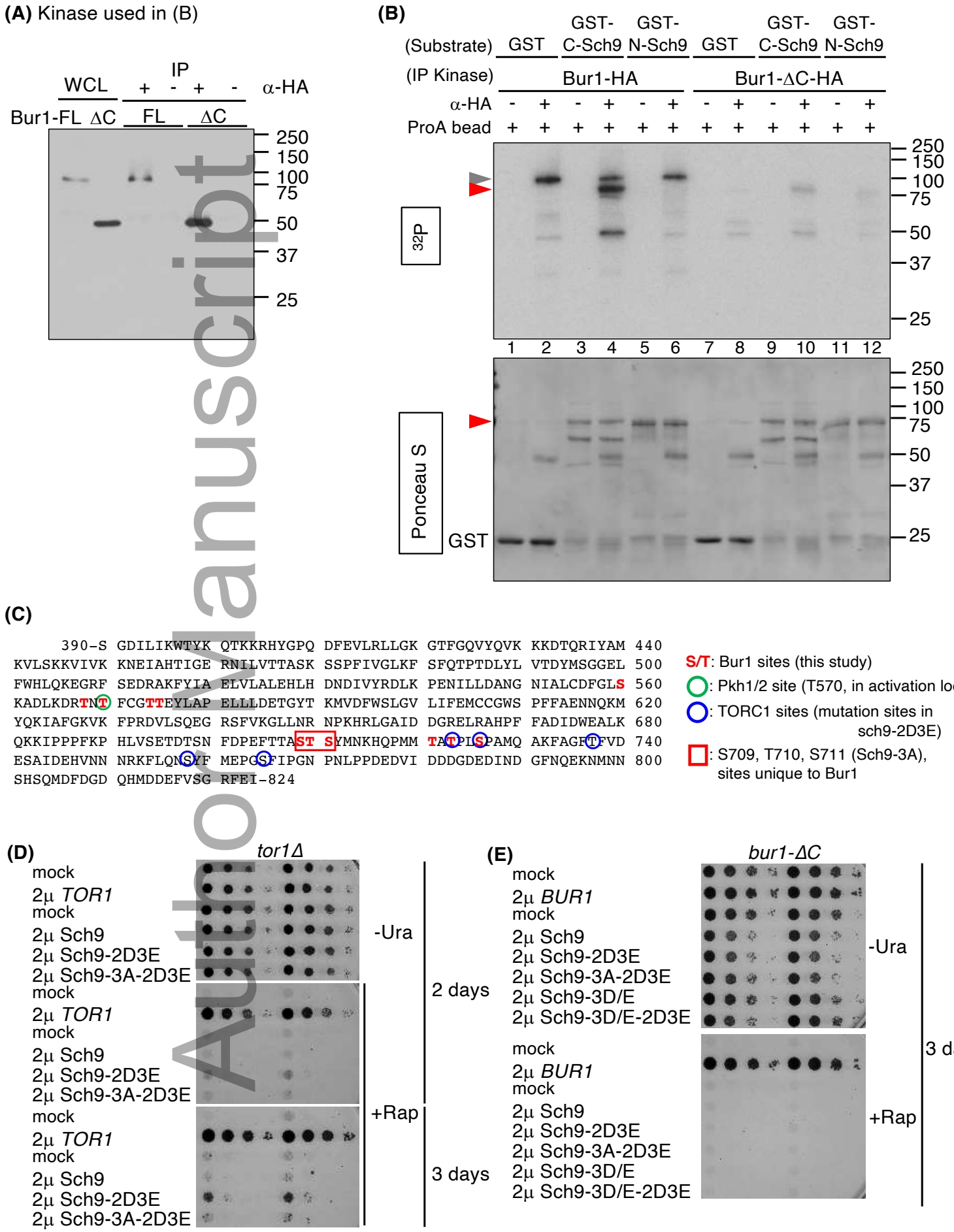

Figure 5. Bur1 phosphorylates Sch9 *in vivo* and *in vitro*.

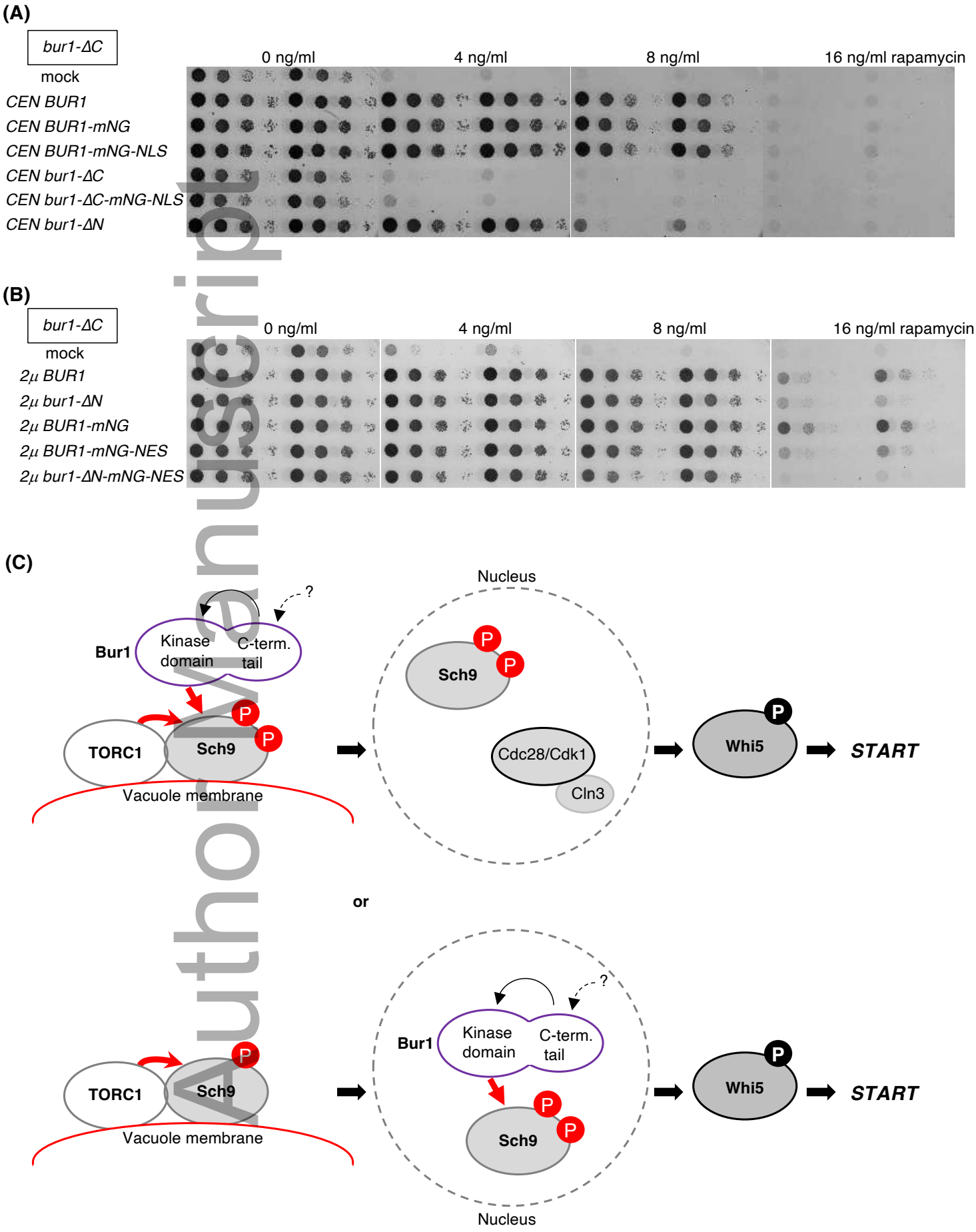

Figure 6. Bur1 functions at the nucleus for TORC1 pathway.